



## Survey Paper

## Advances in Quantum Machine Learning and Deep Learning for Image Classification: A Survey

Ruba Kharsa <sup>a,\*</sup>, Ahmed Bouridane <sup>b</sup>, Abbes Amira <sup>a</sup><sup>a</sup> Department of Computer Science, University of Sharjah, Sharjah, United Arab Emirates<sup>b</sup> Department of Computer Engineering, University of Sharjah, Sharjah, United Arab Emirates

## ARTICLE INFO

Communicated by X. Gu

## Keywords:

Quantum Image Classification  
 Quantum Support Vector Machine  
 Quantum K Nearest Neighbor  
 Quantum Convolutional Neural Network  
 Variational Quantum Circuit  
 Quantum Tensor Network

## ABSTRACT

Image classification, which is a fundamental element of Computer Vision (CV) and Artificial Intelligence (AI), has been researched intensively in numerous domains and embedded in many products. However, with the exponential increase in the number of images and the complexity of the required tasks, deep-learning classification algorithms demand more intensive resources and computational power to train the models and update the massive number of parameters. Quantum computing is a new research technology with a promising capability of exponential speed up and operational parallelization with its unique phenomena including superposition and entanglement. Researchers have already started utilizing Quantum Deep Learning (QDL) and Quantum Machine Learning (QML) in image classification. Yet, to our knowledge, there exists no comprehensive published literature review on quantum image classification. Therefore, this paper analyzes the advances in this field by dividing the studies based on a unique taxonomy, discussing the limitations, summarizing essential aspects of each research, and finally, emphasizing the gaps, challenges, and recommendations. One of the key challenges presented in the paper is that quantum computers are in the Noisy Intermediate-Scale Quantum (NISQ) era, where they contain a limited number of noisy qubits, therefore challenging complex quantum classifiers and complex images from advanced datasets. This research recommends constructing a novel quantum image encoding method that adapts to the available number of qubits and enables RGB images as a critical contribution to the existing research.

## 1. Introduction

Quantum Computing (QC) is an active and promising research area that enables the possibility of developing a new era of computers (i.e., quantum computers). Quantum computers have the potential to overcome the current limitations of classical computers, speed up operations which current computers need more than the time of the universe to achieve, and assist physicists in unfolding the mysteries of quantum physics by providing simulators that are impossible to create, even with the use of the most advanced supercomputers [1]. The latent potentials of quantum computers influenced the major computing and cloud companies (e.g., IBM, Google, Amazon, and Microsoft) to invest in QC research and attempt to create their own quantum computers [2]. Cloud companies also created QC simulators that run on classical computers and programming libraries to aid aspiring researchers in exploring and participating in the expansion and development of QC studies [3,4].

Image classification, segmentation, and detection [5–7] are essential aspects of Computer Vision (CV) that made a revolution in Artificial

Intelligence (AI) applications and allow the construction of systems that benefit humans in daily life and professional tasks. Due to the impact and influence of these fields on human lives, this research reviews the improvement that Quantum holds in these domains.

Over the last decades, computers continued to develop in terms of speed and performance while decreasing in size. That is in agreement with what Moore anticipated fifty-seven years ago back in 1965. Moore stated that the transistors on the Integrated Circuit (IC) and the microchips would double every 18 months [8]. As Moore predicted, the transistors decreased in size over the years until they almost reached the atomic level. This year, IBM has proclaimed that it developed a 2 nm technology that enables 50 billion transistors to be aggregated on a microchip. The actual size of a silicon atom is around 0.2 nm, which means that the current transistors are almost ten times the size of a silicon atom. However, with the transistor reaching atomic size, they start following the quantum rules from quantum physics and exhibit strange behavior that is not explainable by classical physics. Classical computers are at their limit of evolution thus emphasizing

\* Corresponding author.

E-mail addresses: [U21103616@sharjah.ac.ae](mailto:U21103616@sharjah.ac.ae) (R. Kharsa), [abouridane@sharjah.ac.ae](mailto:abouridane@sharjah.ac.ae) (A. Bouridane), [aamira@sharjah.ac.ae](mailto:aamira@sharjah.ac.ae) (A. Amira).

Abbreviations		
Adam	Adaptive Moment Estimation	
AI	Artificial Intelligence	
ANN	Artificial Neural Network	
AQSP	Approximation Quantum State Preparation	
CNN	Convolutional Neural Network	
FC	Fully Connected	
GD	Gradient Descent	
K-L	Karhunen–Loeve	
MERA	Multi-scale Entanglement Renormalization Ansatz	
MPS	Matrix Product State	
mRMR	Minimum Redundancy Maximum Relevance	
MSE	Mean Squared Error	
NISQ	Noisy Intermediate-Scale Quantum	
PCA	Principle Component Analysis	
PQC	Parameterized Quantum Circuit	
QA	Quantum Annealing	
QC	Quantum Computing	
QCNN	Quantum Convolutional Neural Network	
QDL	Quantum Deep Learning	
QKNN	Quantum K Nearest Neighbor	
QML	Quantum Machine Learning	
QNN	Quantum Neural Network	
QSVM	Quantum Support Vector Machine	
QTN	Quantum Tensor Network	
QuanvNN	Quanvolutional Neural Network	
QUBO	Quadratic Unconstrained Binary Optimization	
RMSprop	Root Mean Squared Propagation	
SGD	Stochastic Gradient Descent	
TTN	Tree Tensor Network	
VCNN	Variational Convolutional Neural Network	
VQC	Variational Quantum Circuit	
VQDNN	Variational Quantum Deep Neural Network	
VQTN	Variational Quantum Tensor Network	

the importance of QC in finding opportunities in today's challenges by exploiting the power of quantum mechanics and the behavior of atomic particles (e.g., electrons and photons) to benefit computer applications. Quantum Machine Learning (QML) and Quantum Deep Learning (QDL) [9] are some of the most popular QC applications, especially with the increasing complexity of the ML and DL algorithms to accomplish more accurate and dependable systems. QML and QDL algorithms development can enable parallel tasks and reduce the time complexity of the classical algorithms.

Due to the recent rapid growth in the literature of quantum research, several survey studies have targeted various fields in quantum, like quantum cryptanalysis [10], QML and QDL algorithms and approaches. For QML and QDL, some surveys have focused on implemented quantum algorithms without targeting particular applications or use cases [11–16]. On the other hand, some others have reviewed more specific topics within the field like QML utilization in the biomedical domain [17], quantum optimization [18], quantum software, platforms, and tools [4,19], noise-aware quantum algorithms [20], quantum image representations and processing [21–23], security of QML [24], hybrid quantum–classical algorithms [25,26], quantum classification [27], and quantum annealing [28]. However, to the best of our knowledge, the literature lacks a comprehensive

review of QML and QDL algorithms for image classification, even though researchers conduct intensive studies that employ various quantum algorithms and techniques to classify images. Therefore, this gap demonstrates the need for thorough research that summarizes the approaches and limitations of related papers, compares them, examines the challenges, highlights the openings, and recommends future directions by suggesting possible works to extend the experiments and contribute to the research area.

This paper explores the field of quantum image classification and derives key observations and essential knowledge by addressing new research questions that define the novelty and necessity of the research. Accordingly, the study answers the following questions.

1. What are the different strategies used in the literature to achieve quantum image classification?
2. What are the possible categorizations that divide the employed methodologies?
3. What are the image encoding techniques, model types, quantum algorithms, cost functions, and optimizers utilized in the previous research?
4. What are the key challenges and hurdles when classifying images with QML and QDL?
5. What is the possible future work regarding quantum image classification?

The rest of the paper proceeds as follows. Section 2 introduces the essential knowledge of quantum computing. Section 3 presents the research methodology and paper collection strategy. Section 4 summarizes and categorizes the chosen papers based on the quantum algorithm and explores the image encoding techniques. Moreover, it utilizes summary tables and illustrations to convey the essential knowledge in an easy-to-follow approach. Subsequently, Section 5 analyzes the findings from the previous section to uncover the critical challenges related to quantum image classification and proposes potential advances and future directions. Finally, Section 6 concludes the study with significant discoveries and observations.

## 2. Background of quantum computing

### 2.1. Quantum bits

Quantum bits (Qubits) are analogous to classical bits, which are the basic units of computations. Although bits can only be a 0 or a 1, qubits on the other hand can be in state 0, state 1, or any combination of these two states. The ability of qubits to be in multiple states simultaneously is called superposition. There are  $2^n$  combinations associated with  $n$  bits, yet, with  $n$  qubits, a state can be in a superposition of these  $2^n$  combinations simultaneously. Measurement is an action that collapses the quantum state into one of the basis states with different probabilities. After measuring the qubits, they behave like classical bits, as illustrated in Fig. 1.

Two of the basis qubit states are  $\vec{0}$  and  $\vec{1}$  (1) (2).

$$\vec{0} = \begin{bmatrix} 1 \\ 0 \end{bmatrix} \quad (1)$$

$$\vec{1} = \begin{bmatrix} 0 \\ 1 \end{bmatrix} \quad (2)$$

We can write any 2-dimensional complex vector belonging to the  $\mathbb{C}^2$  space as a linear summation of  $\vec{0}$  and  $\vec{1}$  as shown in (3). Where  $\psi$  is a state-vector in a superposition between 0 and 1 with  $|\alpha^2|$  probability of measuring 0 and  $|\beta^2|$  possibility of measuring 1.  $\alpha$  and  $\beta$  are called probability amplitudes which are distinct from the original probability because they are complex numbers that can take negative values (i.e., from -1 to 1), unlike probabilities that can only have positive values (i.e., from 0 to 1). Therefore, to find the probabilities, the amplitudes are squared. The probabilities of measuring 0 and 1 are

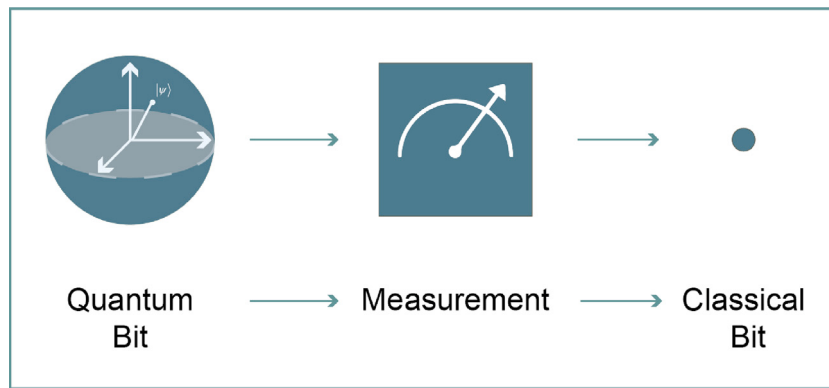


**Fig. 1.** Qubit measurement [1].

mutually exclusive and exhaustive. Thus, the sum of the possibilities should equal  $1 - \alpha^2 + \beta^2 = 1$ .

$$\bar{\psi} = \begin{bmatrix} \alpha \\ \beta \end{bmatrix} = \alpha \begin{bmatrix} 1 \\ 0 \end{bmatrix} + \beta \begin{bmatrix} 0 \\ 1 \end{bmatrix} \quad (3)$$

Entanglement is another concept associated with multi-qubit systems. When two qubits are entangled, measuring one qubit affects the state of the other qubit regardless of the space between them.

## 2.2. Dirac notation

QC uses the bra-ket notation (i.e., Dirac notation) [29]. In Dirac notation a vertical vector  $\vec{v}$  is notated as  $|v\rangle$  and is called ket. Likewise,  $\vec{0}$  is written as  $|0\rangle$ ,  $\vec{1}$  as  $|1\rangle$ , and  $|\psi\rangle = \alpha|0\rangle + \beta|1\rangle$ . The complex conjugate transpose of the ket is the bra, written as  $\langle\psi|$ . The ket and the bra are joined, to form the bra-ket,  $\langle\psi|$  (i.e., the inner product), which is analogous to the dot product. The outer product is calculated by swapping the bra and ket  $|\psi\rangle\langle\psi|$ . The outer product multiplies two vectors to output a matrix, which is useful when representing matrices as a combination of bras and kets. Another state vector multiplication type is the tensor product. The tensor product assists in merging vector spaces and creating vast ones. Also, it allows the use of multiple qubits. (e.g.,  $|0\rangle^{\otimes n}$  represents  $n$  qubits in state 0) [1].

## 2.3. Bloch sphere

The Bloch sphere shown in Fig. 2 allows for the understanding of additional representations of the qubit state-vectors as they provide the conversion of the vector-state from the two-dimensional complex-space  $\mathbb{C}^2$  to a three-dimensional real vector space  $\mathbb{R}^3$  using two angles  $\theta$  and  $\phi$  (4) [1].

$$|\psi\rangle = \cos\frac{\theta}{2}|0\rangle + \sin\frac{\theta}{2}e^{i\phi}|1\rangle \quad (4)$$

## 2.4. Quantum gates

Quantum gates are the method for qubit manipulation. Quantum gates are unitary matrices that act on the qubit vector states and manipulate them. Unitary matrices ensure that the sum of probabilities is enclosed and conserved. Another property of a unitary matrix is that it results in the identity matrix when multiplied by its complex conjugate transpose (5).

$$UU^\dagger = I \quad (5)$$

Fig. 3 illustrates the prevalent single and 2-qubit quantum gates, their matrix representations, and their purposes [30]. The Hadamard gate (H) and the Control-NOT (CNOT) are known to create superposition and entanglement, respectively.

## 2.5. Parameterized quantum circuits

Parameterized Quantum Circuit (PQC) [31], also known as ansatzes, are unitary matrices that vary depending on a set of parameters. The PQC are fundamental components in many quantum algorithms including VQC, QTN, and QCNN. PQC involve a sequence of quantum gates, some are fixed, while the others are parameterized with a set of parameters that may indicate the rotation angles of qubits. Fig. 4 shows the matrix of a few parameterized rotation gates. All single qubit gates, including the rotation gates, can be represented with the most general universal gate in (6) by providing the suitable  $\theta, \phi, \lambda$ .

$$U(\theta, \phi, \lambda) = \begin{pmatrix} \cos\left(\frac{\theta}{2}\right) & -e^{i\lambda}\sin\left(\frac{\theta}{2}\right) \\ e^{i\phi}\sin\left(\frac{\theta}{2}\right) & e^{i(\phi+\lambda)}\cos\left(\frac{\theta}{2}\right) \end{pmatrix} \quad (6)$$

## 3. Research methodology

### 3.1. Literature search

Four top databases (i.e., IEEE Xplore, ACM, Springer Link, and Elsevier) have been searched for recent papers published between 2015 and 2022. “Quantum, Machine Learning, Image, Classification, QCNN, VQC, Quantum Neural Network (QNN), QTN, QSVM, QKNN, and MNIST” are the keywords that have been entered in the advanced search engine to find journal publications and conference proceedings. Since quantum image classification is still a new task, the most used dataset in the research is the MNIST dataset [32] due to its images’ small size (i.e.,  $28 \times 28$  px), hence the use of the “MNIST” keyword.

At the beginning of the process, 85 papers were collected. However, after removing 10 old articles (i.e., published before 2015) and 10 duplicates, then excluding 38 research articles based on the title, abstract, and full paper screening, 27 eligible papers remained and were selected to be reviewed in this study. Fig. 5 illustrates the adopted methodology for choosing the reviewed research.

## 4. Overview of quantum machine learning and quantum deep learning for image classification

This section clarifies the steps and the methodologies for effective image classification using qubits, quantum gates, and quantum circuits. First, the common approaches for data encoding transformation block, which converts the classical images are explained and illustrated, and then the researcher’s diverse approaches are divided based on the quantum classifier algorithms which are constructed based on a QML algorithm like QSVM and QKNN or the hybrid classical-quantum QDL models like the VQC, QTN, and QCNN. In this section (i.e., quantum algorithm), twenty-seven selected research papers are summarized and compared, with their limitations argued to identify the research’s current state and explore the gaps. Fig. 6 visualizes the taxonomy used in this paper.

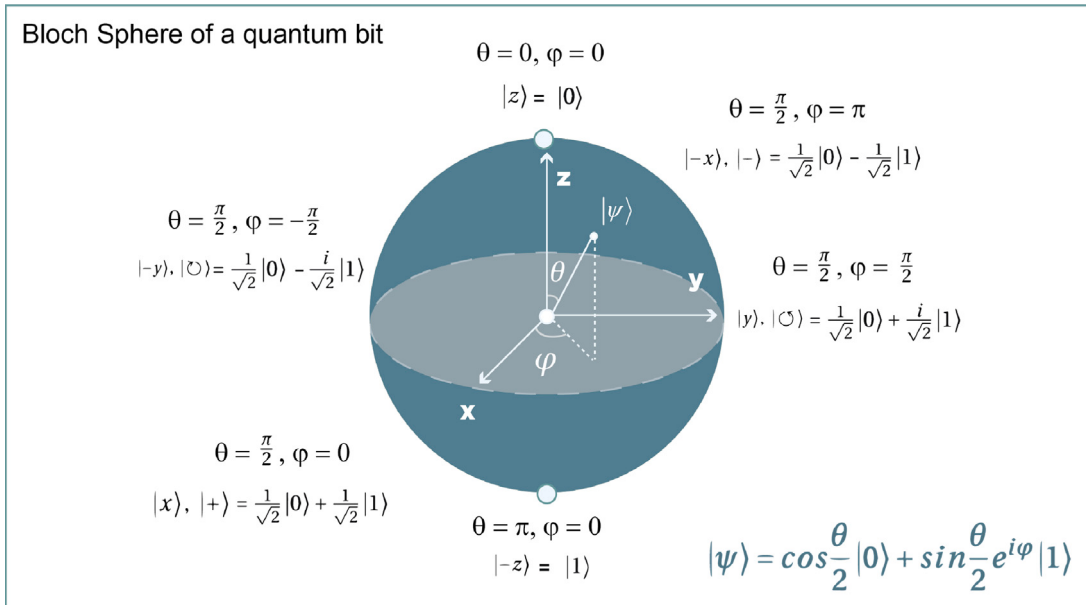


Fig. 2. Qubit (Bloch sphere) vs. bit [1].

Name	Gate(s)	Matrix	Purpose
Pauli-X (X)		$\begin{pmatrix} 0 & 1 \\ 1 & 0 \end{pmatrix}$	- Similar to the Classical Not - Flips the amplitudes of states 0 and 1 - Rotates the state by $\pi$ around the x-axis
Pauli-Y (Y)		$\begin{pmatrix} 0 & -i \\ i & 0 \end{pmatrix}$	- Rotates the state by $\pi$ around the y-axis
Pauli-Z (Z)		$\begin{pmatrix} 1 & 0 \\ 0 & -1 \end{pmatrix}$	- Adds a global phase of -1 to the 1 state - Rotates the state by $\pi$ around the z-axis
Hadamard (H)		$\frac{1}{\sqrt{2}} \begin{pmatrix} 1 & 1 \\ 1 & -1 \end{pmatrix}$	- Converts between the z and x basis - Creates superposition
Phase Shift P( $\varphi$ )		$\begin{pmatrix} 1 & 0 \\ 0 & e^{i\varphi} \end{pmatrix}$	- Adds a global phase of $e^{i\varphi}$ to the 1 state
Controlled Not (CNOT, CX)		$\begin{pmatrix} 1 & 0 & 0 & 0 \\ 0 & 1 & 0 & 0 \\ 0 & 0 & 0 & 1 \\ 0 & 0 & 1 & 0 \end{pmatrix}$	- Performs an X gate on the target qubit if the control qubit is 1
Controlled Z (CZ)		$\begin{pmatrix} 1 & 0 & 0 & 0 \\ 0 & 1 & 0 & 0 \\ 0 & 0 & 1 & 0 \\ 0 & 0 & 0 & -1 \end{pmatrix}$	- Performs a Z gate on the target qubit if the control qubit is 1
SWAP		$\begin{pmatrix} 1 & 0 & 0 & 0 \\ 0 & 0 & 1 & 0 \\ 0 & 1 & 0 & 0 \\ 0 & 0 & 0 & 1 \end{pmatrix}$	- Swaps the states of two qubits
Toffoli (CCNOT, CCX)		$\begin{pmatrix} 1 & 0 & 0 & 0 & 0 & 0 & 0 & 0 \\ 0 & 1 & 0 & 0 & 0 & 0 & 0 & 0 \\ 0 & 0 & 1 & 0 & 0 & 0 & 0 & 0 \\ 0 & 0 & 0 & 1 & 0 & 0 & 0 & 0 \\ 0 & 0 & 0 & 0 & 1 & 0 & 0 & 0 \\ 0 & 0 & 0 & 0 & 0 & 0 & 1 & 0 \\ 0 & 0 & 0 & 0 & 0 & 0 & 0 & 1 \\ 0 & 0 & 0 & 0 & 0 & 1 & 0 & 0 \end{pmatrix}$	- Performs an X gate on the target qubit if both control qubits are 1

Fig. 3. Common quantum gates [30].

Name	Gate	Matrix
Parameterized X Rotation	$R_x(\theta)$	$\begin{pmatrix} \cos(\theta/2) & -i \sin(\theta/2) \\ -i \sin(\theta/2) & \cos(\theta/2) \end{pmatrix}$
Parameterized Y Rotation	$R_y(\theta)$	$\begin{pmatrix} \cos(\theta/2) & -\sin(\theta/2) \\ \sin(\theta/2) & \cos(\theta/2) \end{pmatrix}$
Parameterized Z Rotation	$R_z(\phi)$	$\begin{pmatrix} e^{-i\phi/2} & 0 \\ 0 & e^{i\phi/2} \end{pmatrix}$

Fig. 4. Parameterized rotational quantum gates [1].

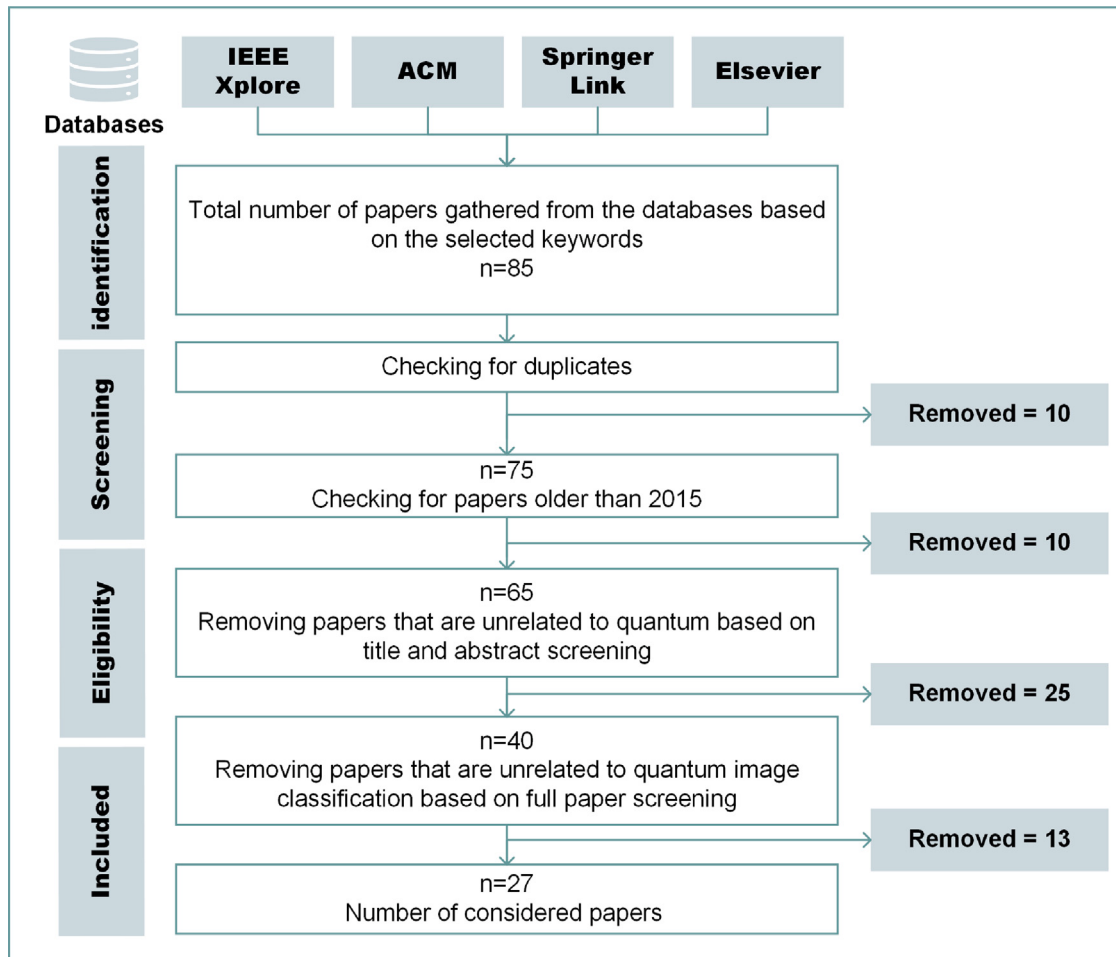


Fig. 5. Research methodology.

#### 4.1. Encoding methods

There are many methods to encode classical images into quantum states. Each method has its strengths and weaknesses. With the limited

number of available qubits in the Noisy Intermediate-Scale Quantum (NISQ) era, the embedding technique can enhance or degrade the quality and efficiency of the overall circuit. Hence, selecting the most appropriate encoding method is one of the critical challenges that researchers are still investigating.

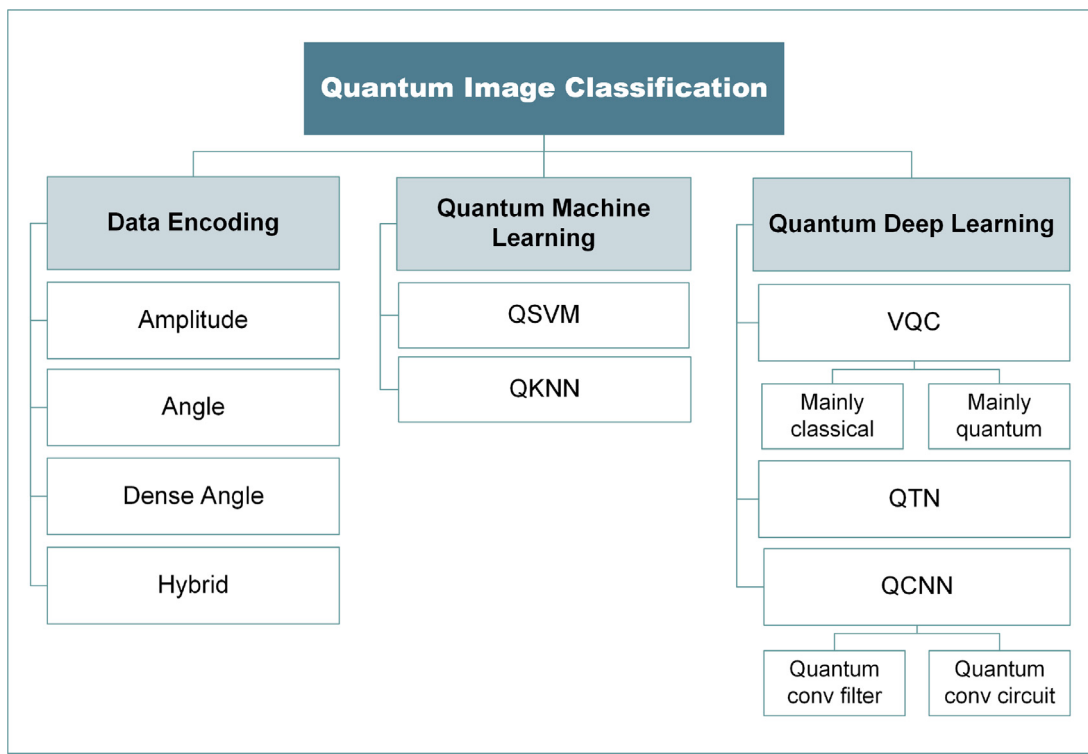


Fig. 6. Taxonomy of the review paper.

#### 4.1.1. Amplitude encoding

As discussed in Section 2.1,  $n$  qubits can have  $2^n$  amplitudes. Thus, the amplitudes can be employed to encode the image pixels using a practical number of qubits. Let a classical image array of  $N$  pixels be  $[X_1, X_2, \dots, X_N]$ , then the number of qubits to embed the array is  $n = \log_2(N)$ . The resulting quantum state is shown in (7). The  $\frac{1}{\sum_{i=1}^N \|X_i\|}$  is the normalizing factor because the sum of the probabilities (i.e., the square of the amplitudes) for all bases should be 1.

$$|\psi\rangle = \frac{1}{\sum_{i=1}^N \|X_i\|} (X_1 |0_1 0_2 \dots 0_n\rangle + \dots + X_N |1_1 1_2 \dots 1_n\rangle) \quad (7)$$

The main advantage of amplitude embedding relates to the efficient number of qubits used, as the number of the required qubits is  $O(\log_2(N))$  where  $N$  is the number of classical data points, but the main limitation results from the computational complexity and the circuit depth required for the quantum state. The circuit depth is the number of quantum gate layers that can be performed in parallel. Also, it is the longest path in the circuit. The circuit depth scales exponentially with the number of qubits (i.e.,  $O(2^n)$  for  $n$  qubits) in amplitude encoding [33–36].

#### 4.1.2. Angle encoding

The angle embedding encodes image pixels as rotation angles using one of the parameterized rotation gates in Fig. 4. The pixels are converted into angles using some transformation. (e.g., let  $X$  be a flattened image and  $x_i \in X$  corresponds to the  $i$ th pixel, then  $\theta_i$  can be  $\pi * x_i$ ). The resulting quantum state  $|X\rangle$  is calculated using (8), where  $R$  is a parameterized rotation gate and  $n$  is the number of qubits.

$$|X\rangle = R(\theta_1) |0\rangle \otimes R(\theta_2) |0\rangle \otimes \dots \otimes R(\theta_n) |0\rangle \quad (8)$$

The main advantage of using angle encoding is that the depth of the circuit is shallow and has constant complexity  $O(1)$ , as we only use one gate at each qubit. However, the major constraint is that the angle encoding needs as many qubits as the number of image pixels. Let the image array consist of  $N$  pixels, then  $O(N)$  qubits are required. Meaning, the  $|X\rangle$  would have  $O(2^N)$  amplitudes. Therefore, simulators

in classical computers can only handle encoding a few pixels since the size of the amplitudes that they need to keep track of increases exponentially.

#### 4.1.3. Dense angle encoding

Dense angle encoding is introduced as a solution, where it encodes two pixels in each qubit. It reduces the required qubits to  $N/2$ , thus the amplitudes of the quantum state are reduced to  $O(2^{N/2})$  [35–39]. (9) depicts an example of dense encoding, where the second pixel in each qubit is encoded using the phase shift gate  $P$ .

$$|X\rangle = R(\theta_1)P(\theta_2) |0\rangle \otimes \dots \otimes R(\theta_{n-1})P(\theta_n) |0\rangle \quad (9)$$

#### 4.1.4. Encoding experiment

To further analyze the performance of each encoding method, an experiment is done using the PennyLane Python library [40].

A vector  $X = [x_0, x_1, \dots, x_N] \in \mathbb{R}^N$  is defined, where  $x_i \in X \in \mathbb{R}$  is a random real number. In the first step,  $N$  is assigned to 1. Then it is doubled until we get  $N = 64$ . As a preprocessing for amplitude encoding, each value  $x_i$  is normalized using (10) to ensure that the resulting probabilities sum to 1 as discussed earlier. However, the normalization step is not considered in testing. The same normalized vector is used for all the encoding methods.

$$\|x_i\| = \frac{x_i}{\left(\sum_{j=0}^N |x_j|^2\right)^{\frac{1}{2}}} \quad (10)$$

The amplitude encoding is achieved using the Mottonen state preparation method [41]. The angle encoding is implemented by rotating each qubit  $i$  by  $x_i$ . Lastly, the dense angle encoding is done by using the rotational gate  $R_y(x_i)$  and the phase shift gate  $P_{x_{i+1}}$  on qubit  $i$ .

The execution time of the quantum state preparation is recorded for each method. To ensure consistency, an average of 100 executions is taken at each step. The results are shown in Fig. 7. The results show an approximately linear relationship between the state preparation time and the vector length  $N$  in the amplitude encoding. The amplitude encoding outperformed the angle and the dense angle for larger  $N$ . In

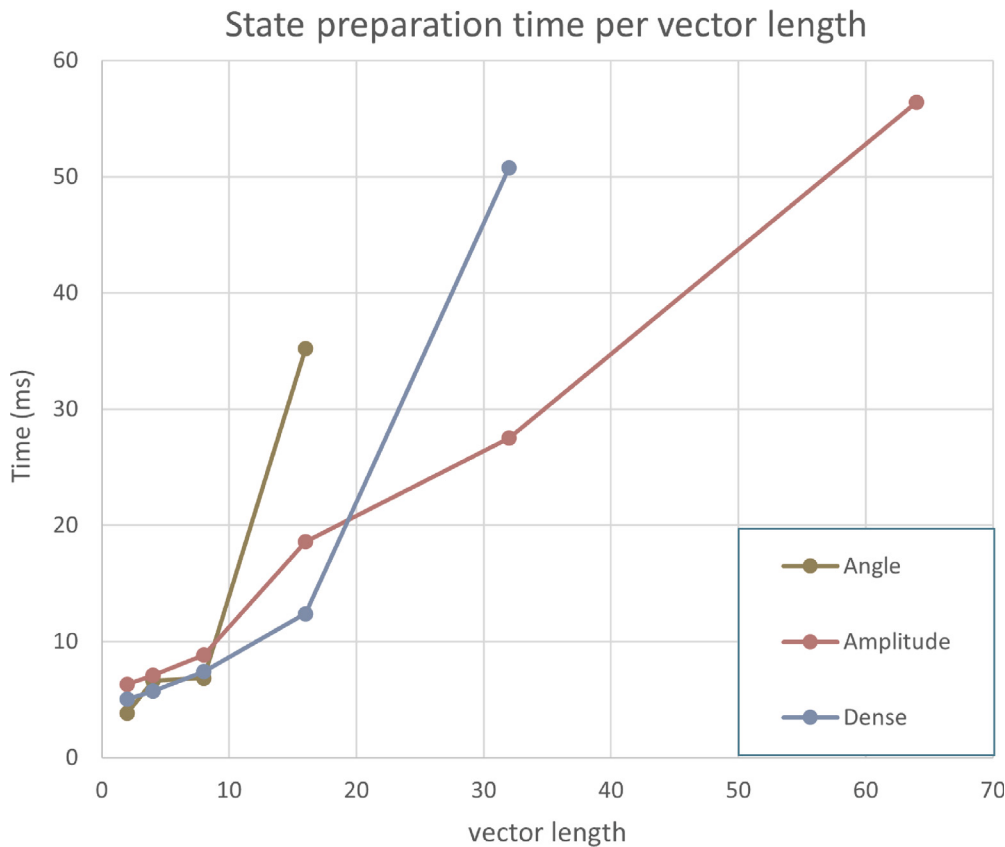


Fig. 7. State preparation time per vector length.

fact, the angle encoding method could not be achieved by the used environment for  $N \geq 32$ . This is as discussed due to the enormous number of amplitudes that result from using 32 and 64 qubits. As for the dense angle method, it was able to accommodate the  $N = 32$  but failed for  $N = 64$ . As can be seen from the graph, the angle and dense encoding performance decrease as the number of qubits increases. For a more comprehensive overview, the actual resulting circuits for the quantum state preparation are shown in Fig. 8. The figure highlights the complexity and the issues of each encoding method. As the figure shows the depth of the state preparation circuit exponentially increases with the number of qubits in the amplitude encoding method. As for angle encoding the main issue is that the number of qubits linearly increases with  $N$ .

Tables 1 and 2 summarize the findings from Fig. 8 and then report the computational complexity of each method using the big  $O$  notation. In amplitude encoding, the depth of the circuit with respect to the vector length  $N$  is analyzed in three steps. First, the number of quantum layers that contain  $R_Y$  and CNOT gates are counted in each circuit. Then the total depth is calculated as the sum of both layers. After that, the functions  $F(N)$  for calculating the  $R_Y$ , CNOT, and the total depth are derived to interpret the complexity. To simplify the task, the functions were derived with respect to the number of qubits first, then mapped to the corresponding ones for the vector length. Suppose  $n$  is the number of qubits, then the required number of CNOT layers in the circuit are equal to  $2^n - 2$  and the  $R_Y$  layers are  $2^n - n$ . This means that the total depth with respect to  $n$  is  $2^{n+1} - n - 2$  and that proves that the depth of the circuit has  $O(2^n)$ , where  $n$  is the number of qubits. However, the main point of this study is to check the image encoding complexity. Therefore, the complexities are reported with respect to the vector length. As our assumption,  $N$  can only be a power of 2 and it is the square of the number of qubits  $n$ . Therefore,  $n = \log_2(N)$  can be substituted in the formulas to get the formulas shown in the table, where  $N-2$  CNOT gates are required for  $N$  pixels or points,  $N-\log_2(N)$

for  $R_Y$  layers, and  $2N - \log_2(N) - 2$  for the total depth, which means the total depth is linear with the number of points  $O(N)$ . As for the resulting amplitudes, they will equal  $N$  as each amplitude represents one point. As for the angle encoding, the number of amplitudes in the resulting quantum state is doubled with each additional pixel making it unfeasible for large  $N$  in the current NISQ era.

#### 4.1.5. Hybrid encoding

Researchers have designed more advanced encoding methods that involve the characteristics from both amplitude and angle strategies to reduce the number of qubits and gates, thus reducing the circuit complexity and increasing the algorithm efficiency [35,36].

Fig. 9 depicts the schemes of amplitude, angle, and dense angle encodings in the image classification task. First, the image is reduced in size to accommodate the current capabilities of simulators, then it is converted to a flattened array of pixels. This can be done by sliding a kernel of size  $F \times F$  across the image to flatten the pixels, or the pixels can be flattened row by row. Then the array is entered into the quantum preparation circuit using one of the examined approaches. To summarize, amplitude encoding requires fewer qubits but more circuit depth. On the other hand, angle encoding demands more qubits but fewer transformation gates. Finally, dense angle encoding balances the two extremes with shorter length and shallower depth.

## 4.2. Quantum machine learning algorithms

### 4.2.1. Quantum support vector machine

Delibasic et al. [42] proposed a QSVM to remote sensing classification. The SemCity Toulouse dataset [43] was selected containing multi-spectral images of Toulouse city in France. The performed task is the segmentation of the building areas in each image. Yet, the primary problem is binary classification, as the model classifies each pixel based on whether it contains a building or not. The proposed QSVM algorithm

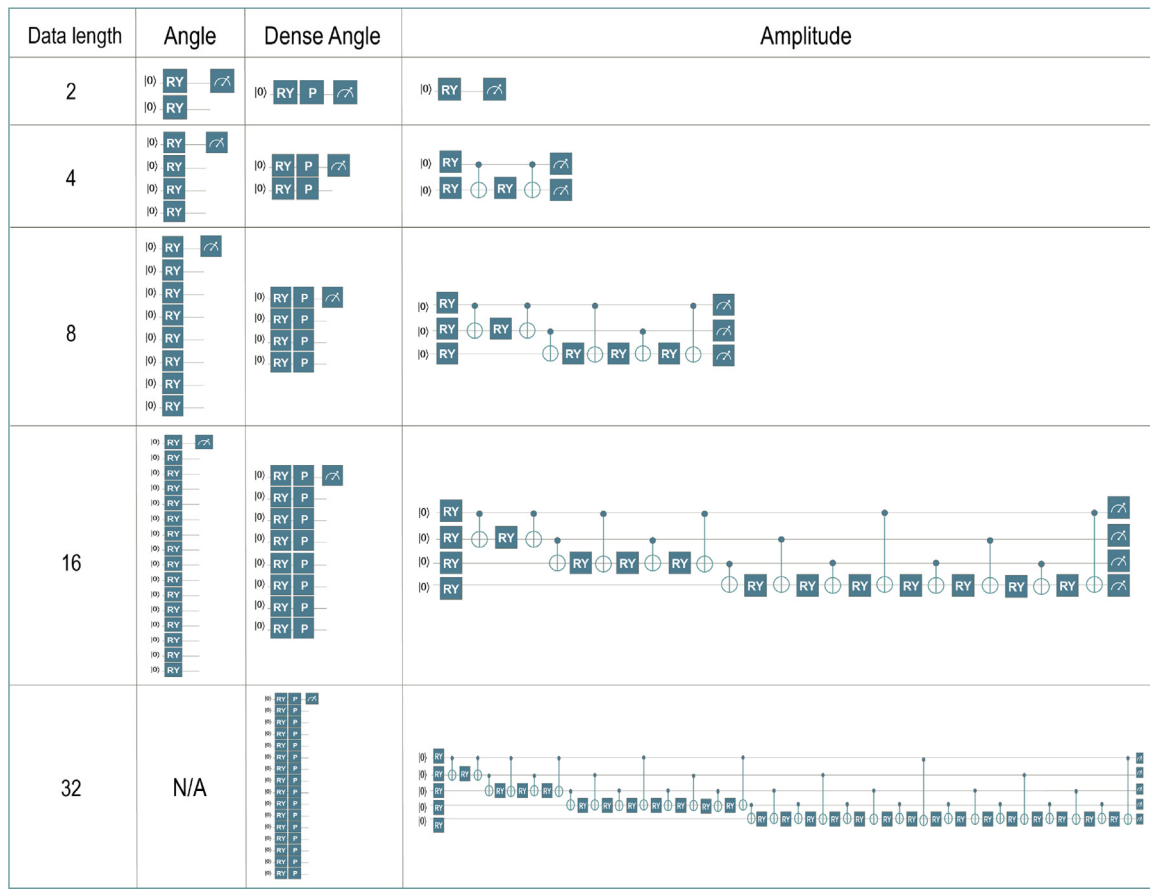


Fig. 8. The resulting state preparation circuits with respect to the vector length.

**Table 1**  
Results of the amplitude encoding.

Vector length (N)	Amplitude				Resulting amplitudes	
	Required qubits	Circuit depth				
		CNOT layers	RY layers	Total		
2	1	0	1	1	2	
4	2	2	2	4	4	
8	3	6	5	11	8	
16	4	14	12	26	16	
32	5	30	27	57	32	
64	6	62	58	120	64	
F(N)	$Q = \log_2(N)$	$C NOT = N - 2$	$R_Y = N - \log_2(N)$	$D = 2N - \log_2(N) - 2$	$A = N$	
Big O	$O(\log(N))$	$O(N)$	$O(N)$	$O(N)$	$O(N)$	

**Table 2**  
Results of the angle and the dense angle encoding methods.

Vector length (N)	Angle			Dense		
	Required qubits	Circuit depth	Resulting amplitudes	Required qubits	Circuit depth	Resulting amplitudes
2	2	1	4	1	2	2
4	4	1	16	2	2	4
8	8	1	256	4	2	16
16	16	1	65536	8	2	256
32	32	1	$4.9e^9$	16	2	65536
64	64	1	$1.8e^{19}$	32	2	$4.9e^9$
F(N)	$Q(N) = N$	$D(N) = 1$	$A(N) = 2^N$	$Q(N) = N/2$	$D(N) = 2$	$A(N) = 2^{N/2}$
Big O	$O(N)$	$O(1)$	$O(2^N)$	$O(N)$	$O(1)$	$O(2^{N/2})$

used Quadratic Unconstrained Binary Optimization (QUBO) attempts to employ the Quantum Annealing (QA) [44] principles to the SVM training. The central concept behind the QA is to solve an optimization problem by minimizing the energy of a quantum state. The experiments

are conducted on a real quantum machine using the D-wave platform that contains 5000 qubits, and the IBM platform with 15 qubits. The QSVM is compared to the classical SVM using the accuracy and F1 score. The results show a higher F1 score of the QSVM than the SVM,

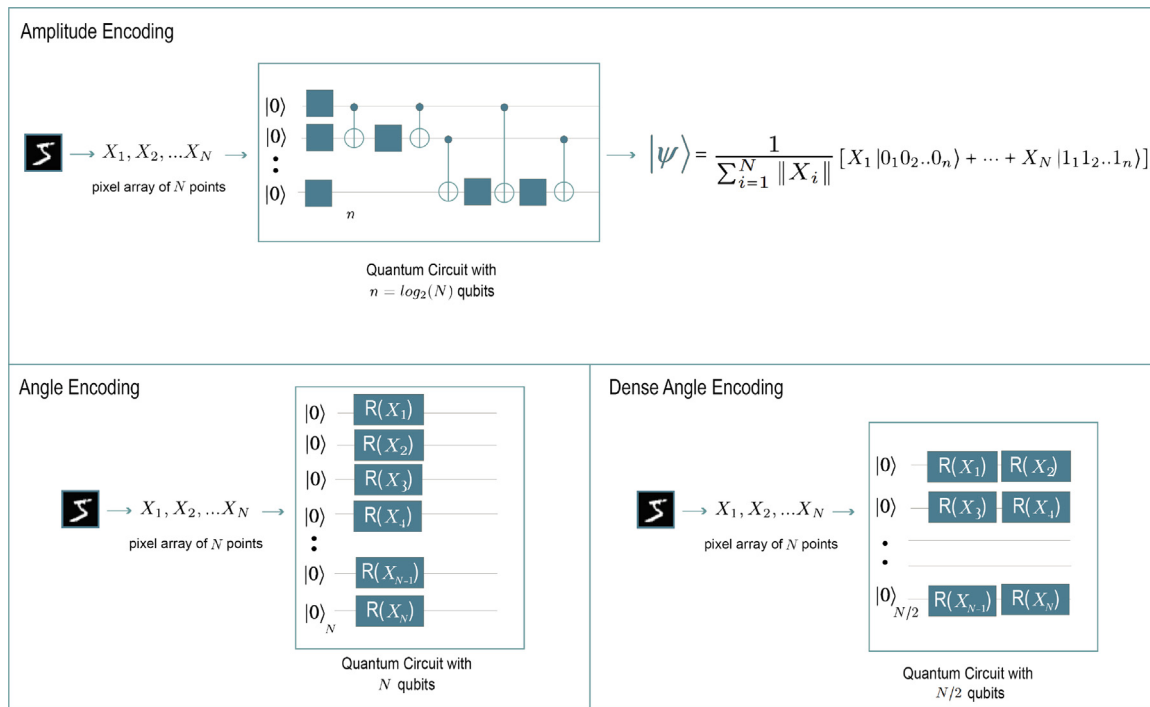


Fig. 9. Amplitude, angle, and dense angle encoding schemes.

**Table 3**  
QSVM papers.

Paper	Dataset	Qubits	Evaluation & Results	Classification type	Limitation
Delilbasic et al. [42]	SemCity Toulouse	15	73.4% ACC	Binary for each pixel	Some qubits in the hardware are not physically connected, which challenges maintaining the logical structure of the problem.
Li et al. [45]	Handwritten digits	4	N/A	Binary	No experiments details or evaluations.

with 73.4% and 69.7%, respectively. The major constraint of the work is that some qubits in the hardware are not physically connected, which challenges maintaining the logical structure of the problem.

Li et al. [45] applied a QSVM algorithm to differentiate between the 6 and the 9 using four qubits and to provide exponential acceleration to the classical SVM. Each image of the chosen numbers is converted to a feature space of two components (i.e., the vertical and horizontal ratios). Then, the feature array is normalized and linearized. The QSVM constructions utilize the Hadamard gate to create a superposition, a matrix inversion, a training state preparation oracle, and a  $U_x$  gate that adds the feature vectors to the quantum circuit. Finally, the output predictions depend on the measurement results of the Ancilla qubit. Nevertheless, no evaluation was carried out in this paper. Based on Li et al. [45] research, Rana et al. [46] conducted a comparative study between the performance of the classical SVM and the QSVM algorithms for handwritten character recognition. The authors examined the advances in both algorithms and reviewed the adopted approaches where it was found that the use of QSVM holds a promising future for ML algorithms and classification tasks as it speeds up operations and improves correctness. Table 3 summarizes the papers that utilize QSVM in their research.

#### 4.2.2. Quantum K nearest neighbor

The QKNN technique allows the parallelization of distance measurements between one observation and a set of instances regardless of the size of the set, using concepts such as superposition and phase kickback. Table 4 shows the main QKNN papers.

Ruan et al. [47] proposed a QKNN by constructing a quantum circuit to calculate the Hamming distance to determine the class of

a new instance based on the most similar training samples. The time complexity of the proposed algorithm only depends on the feature size rather than the number of samples, which increases the model's scalability. The MNIST dataset is utilized for the evaluation phase. The preparation stage for the constructed QKNN starts by extracting the features from the training images using a hash function to convert each image to a binary representation of 64-bit. Each of the bits is mapped to a qubit state based on its value (i.e., 0 to  $|0\rangle$  and 1 to  $|1\rangle$ ). A superposition of all qubits is then created. The testing sample is converted to the quantum state using the same approach. The Hamming distance is measured using a quantum circuit with three registers as follows. The first is the superposition state of the training set, the second is the testing sample, and the third is the ancillary qubit that determines the distance. The k is set to 20 to classify the testing image based on the 20 neighbors. The results show almost 98% accuracy for different training set sizes.

Dang et al. [48] extended the work in [47] with color support using more complex datasets. The authors also implemented another distance metric and reported a  $O(\sqrt{k}M)$  time complexity, where  $M$  is the number of samples in the dataset. The used datasets are the Graz-01 and the Caltech-101 datasets. The RGB color images are converted to HSB (Hue, Saturation, and Brightness) to enable the extraction of the color features. The values of the color system are then split into 8, 3, and 3 categories for H, S, and B, respectively, and aggregated into one value. The texture is also extracted and normalized from the grey-level version of the images based on some criteria (e.g., contrast and correlation). Then, the extracted color and texture features are incorporated into one flattened array. The features 1-D vector is created

**Table 4**  
QKNN papers.

Paper	Encoding	Dataset	Distance metric	Evaluation & Results	Classification type	Limitation
Ruan et al. [47]	Basis	MNIST	Hamming	98% ACC	Multi-class	Could have used more efficient embeddings than the basis encoding like angle or amplitude
Dang et al. [48]	Amplitude	Graz-01 - Caltech-101	Cosine	83.1% ACC on Graz-01 78% ACC on Caltech-101	Binary Multi-class	The feature extraction method of color and texture by aggregating 8, 3, and 3 categories for H, B, and S into one value is quite simplistic.
Wang et al. [49]	Quantum amplitude estimation algorithm	Handwritten digit recognition	Cosine	N/A	Multi-class	No experiments details or evaluations.
Zhou et al. [50]	Basis	MNIST FMNIST CIFAR-10	Hamming	97% on MNIST 90% on FMNIST 51% on CIFAR	Multi-class	Could have used more efficient embeddings than the basis encoding like angle or amplitude

for the training and the testing images. The feature vector of the testing image and the training set are prepared and stored in two quantum states in a superposition to find the distance between the two states. Fidelity is adopted as the distance metric (i.e., cosine similarity) and the quantum circuit for calculating the fidelity has three qubits. The distance between the first two qubits is calculated and the results are obtained using a measurement operation on the third ancillary qubit. First, a Hadamard gate creates a superposition state of the ancillary qubit, then a controlled swap gate uses the superposition of the ancilla as a control to flip the state of the other two qubits only on the  $|1\rangle$  of the ancilla, which creates the phase kickback phenomenon [1] on the state of the ancilla. After the controlled swap gate, another Hadamard gate is appended to allow the Z-measurement of the ancilla. If the two states are similar, there is a 100% chance of measuring 0, and the further the states are from each other, the smaller the probability of |0|. The next step searches for the minimum k values using Grover search and classifying the testing image based on the majority rule. The result of their experiments is an accuracy of 83.1% and 78% on the Graz-01 and Caltech-101 datasets, respectively.

Wang et al. [49] followed a similar approach to Dang et al. [48] to provide an improved QKNN for handwritten digit recognition. The authors initially used superposition concepts to prepare two quantum states,  $\alpha$  and  $\beta$ , for the testing and training sets, respectively. Then they measured the cosine similarity using the same circuit as Dang et al. [48] with the swap and the two Hadamard gates. Once done, the distance is stored in the quantum state amplitudes by converting these amplitudes to the quantum state using a technique called the quantum amplitude estimation algorithm. The top k similar digits to the testing instance are obtained using a search algorithm that utilizes Grover search. Unfortunately, Wang et al. [49] did not provide experiment details or evaluations.

Zhou et al. [50] proposed an enhanced QKNN method that uses the Karhunen–Loeve (K-L) transform for feature extraction from colored and grey images. Similar to Ruan et al. [47], the authors employed Hamming distance as their similarity metrics. After creating the quantum states from the extracted features, measuring the distance using a quantum circuit, and finding the minimum k distances with the Grover search, the majority voting is achieved using distance-weighted voting strategy [51]. The MNIST, FMNIST, and CIFAR-10 datasets are used for experiments and classification. Three experiments with three different k values (i.e., 30, 50, and 70) were performed to select the best k value. The results show that 30 is the best k, and the accuracies are 97% on MNIST, 90% on FMNIST, and 51% on CIFAR. The reported findings achieve 2%, 4%, and 10% relative improvement compared to the classical KNN on the three datasets. Fig. 10 illustrates the general procedure to construct a QKNN based on the previous studies.

#### 4.3. Quantum deep learning algorithms

This section discusses the QDL algorithms and surveys the papers that employ these algorithms as their proposed architecture. The majority of the reviewed papers utilize one of three general approaches

to achieve the QDL on image classification. These are the VQC, the QTN, and the QCNN. All these approaches are hybrid classical-quantum models that combine classical and quantum concepts to achieve image classification, which makes them suitable for implementation in the NISQ era. The main concept behind these approaches is the use of a number of PQCs with trainable parameters. These circuits are trained to minimize the error of the predictions using a classical optimizer after the measurement. The main difference between the VQC and the other two approaches is that the VQC focuses on training a number of PQCs that do not follow a specific classical architecture. VQC can be analog to Artificial Neural Network (ANN) in classical terminology. In contrast, the QCNN is designed in a way that imitates the concept of the classical CNN by incorporating feature extraction capabilities of the convolution layers and the dimensionality reduction in the pooling layers through quantum gates. As for the QTN, it can be considered as the quantum version of the tensor networks.

##### 4.3.1. Variational/parameterized quantum circuit

The VQC approach is widely researched in literature. One strategy is inserting a number of PQCs into a classical model. The classical model can be ANN, CNN, or a CNN-based transfer learning model. Another strategy is building the majority of the trainable model blocks using PQCs. The two approaches are highlighted in Fig. 11

**4.3.1.1. Mainly classical.** Mittal and Dana [52] employed classical to quantum transfer learning to identify the gender from the facial images. They used a pre-trained VGG-16 CNN [53] with a VQC layer. The images are downsampled to  $50 \times 50$  dimension, entered into the VGG-16 pre-trained network followed by a classical layer that reduces the feature size from the VGG-16 network from 25 088 to 4 to fit into a VQC with 4 qubits. Another classical layer proceeds the VQC and further reduces the 4-dimensional resulting data from the VQC into the two classes (i.e., female or male). Their experiments result in a mean test accuracy of almost 93%. However, Mittal and Dana [52] provided little information about the encoding method and the VQC architecture and gates.

Trochun et al. [54] proposed a detection technique of hurricane damage using Hybrid CNN. The Qiskit Simulation platform was utilized for the implementations. The used VQC is a simple two quantum gates (i.e., H and  $R(\theta)$ ) connected to three conv and two Fully Connected (FC) layers. The VQC layer is implemented at the end of the CNN and is connected to a Sigmoid activation function that produces two classes from the qubit measurement. Their accuracy results show that the use of the hybrid model still needs improvement to reach the accuracy of the pure classical CNN model, as the latter has a 4% relative percentage improvement to the hybrid model. The research also discussed the accuracy drop phenomena in the hybrid model as it stops learning after the 15th epoch. Also, the accuracy of experiments dropped from almost 70% to less than 50%.

Sebastianelli et al. [55] constructed a hybrid model with three conv, one flattened, one FC, a VQC, another FC, and finally a softmax layer

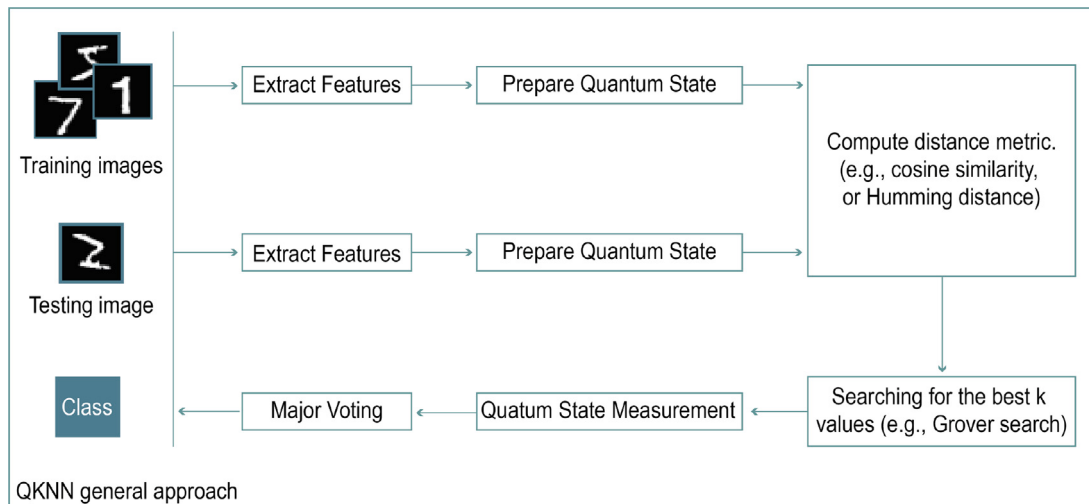


Fig. 10. QKNN general approach [48–50].

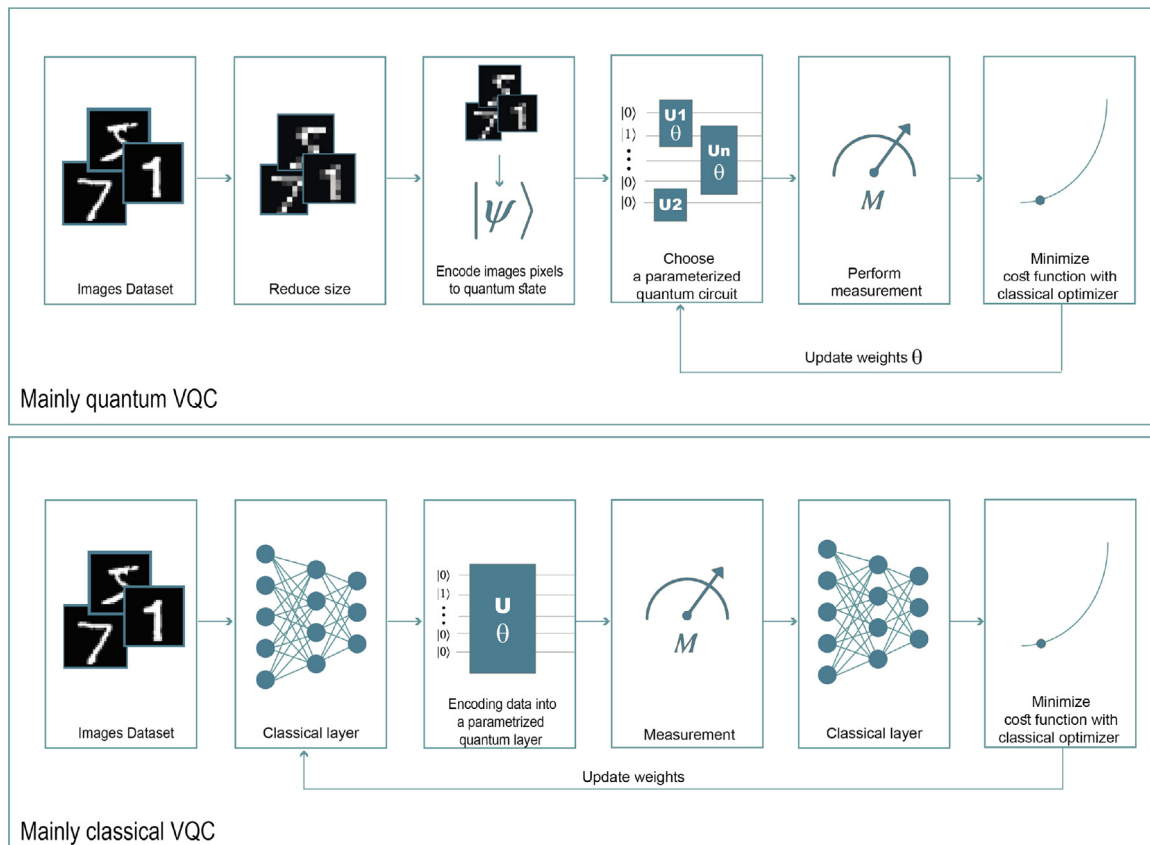


Fig. 11. VQC as a layer in a classical model vs. as the main model.

to classify remote sensing images to 10 classes based on the land type. Three different VQC architectures are investigated and compared. These are No-Entanglement that does not involve any 2-qubit gates, a Bellman that entangles every two successive gates, and a Real-Amplitudes circuit that implements complete entanglement between all the qubits. Extensive experiments are conducted to evaluate the proposed approach. The experiments show that the hybrid model with the real amplitude circuit yields the best results compared to pure classical models and other hybrid models with different VQC. The real amplitude circuit achieved an overall accuracy of 92% compared to purely classical models which reached 83% in the 10-class classification

task. To further analyze the performance of the hybrid model with a real amplitude circuit, another experiment has been conducted. First, the 10 classes are clustered into three macro classes, which are the urban cluster (3 classes), vegetation (5 classes), and water bodies (2 classes). After that, four real-amplitude classifiers are used to perform the final classification. One classifier is trained to classify the input image into one of the three macro-classes, and based on the resulting class, one of the three other classifiers is used to output the final class. The multi-level classification accomplished an overall accuracy of 97%. The authors compared their results to Helber et al. [56] who used the Resnet-50 architecture and achieved an accuracy of 98%. However,

Sebastianelli et al. [55] argued that their hybrid classical-quantum model with the real amplitude VQC is considerably less complex than the Resnet-50 model as the latter uses 50 layers while the proposed model uses only 6 (5 classical and 1 quantum)

Chalumuri et al. [57] executed their experiments on a real quantum computer using the IBM platform to confirm the feasibility of their approach on NISQ computers. They proposed a hybrid model consisting of a quantum feature extraction phase and a classical DNN for classification. The amplitude encoding is employed to encode images from UC Merced Land-Use, AID, and NWPU-RESISC45 datasets using 8, 9, and 7 qubits, respectively. The resulting accuracies of the constructed hybrid architecture are 95.89%, 86.13%, and 79.32% on the three datasets. Chalumuri et al. [57] found that quantum layers in a hybrid model can outperform the state-of-the-art models with almost one-third of the parameters.

Azevedo et al. [58] appended three classical transfer learning models, which are DenseNet-161 [59], ResNet-18 [60], and ResNeXt [61] with a Dressed QuantumNet that contains a VQC for the task of breast cancer binary classification. All parameters from the transfer learning models are freezed and only the Dressed QuantumNet contains trainable parameters that can be fine-tuned. The Dressed QuantumNet is a network with an input that is equal to the number of extracted features from the transfer learning model and an output that is equal to the number of final classes. Inside the Dressed QuantumNet there is a pre-processing layer that projects the number of features that resulted from each transfer learning model to 4 features and applies the tanh activation function. After the number of features is reduced to 4, 4-qubit multi-layered VQC is applied. Each feature  $i$  of the four features is multiplied by  $\pi/2$  and converted to an angle  $\theta_i$  then a Hadamard followed by an  $R_y(\theta_i)$  are performed on each qubit for data encoding. Each layer  $l$  in the VQC consists of three CNOT gates that fully entangle the qubits, and four parameterized  $R_y(w_i)$  where  $w_i$  is a trainable weight corresponding to feature  $i$ . The four qubits are measured at the end of the VQC and 4 classical values are obtained. Finally, these 4 classical values are entered into a post-processing layer that outputs 2 values representing the probability of each class (benign and malignant). The Adaptive Moment Estimation (Adam) classifier is used to optimize the cross-entropy loss function with a decay learning rate. Intensive experiments on a real quantum computer from IBM showed that the Resnet-18 model with an  $l = 1$  layered VQC and 2066 trainable parameters outperformed other models with an accuracy of 84% and AUC of 77.0%.

T et al. [38] adjusted the approach of Mittal and Dana [52] to recognize brain tumors from MRI images. They used the ResNet-18 [60] to extract features, followed by a linear layer to map 512 to 4 features. Then, they encoded the classical reduced feature vector to the qubits using angle encoding. Finally, the VQC is measured to produce 4 classical outputs to the last FC layer that classifies the data into a tumor or healthy MRI image. T et al. [38] reported maximum validation accuracy of 83.66%. Nevertheless, no comparison with the classical model is performed.

**4.3.1.2. Mainly quantum.** Wang et al. [35] proposed three Variational Quantum Deep Neural Network (VQDNN) classifiers, and performed extensive experiments on the MNIST and the UCI datasets for binary and multiclass classification. In the first model, the images are reduced from 784 to 10 pixels in the MNIST dataset, and then the angle encoding method is performed, which results in ten qubits. After data encoding,  $N$  layered VQC of one and two-qubit gates is implemented. Then, the 10 qubits are measured and a classical fully connected layer is implemented for the final classification task. In the second model, the images are padded until the total number of pixels are power of 2. (1024 pixels for MNIST and 64 for UCI). The pixels are then encoded using the amplitude encoding method where the number of qubits are 10 and 8 for the MNIST and the UCI, respectively. After the data preparation method, the same architecture as the first model

is implemented. In the third architecture, a hybrid encoding model is implemented where the first model is appended to the end of the second one. The amplitude encoding and the multi-layered VQC are used as the first part of the model, and then the classical results of the qubit measurement are re-encoded using the angle encoding method which is followed again by the same architecture. Diverse classification tasks are performed and compared with classical ANNs that have a similar number of parameters. The experiment results favor the VQDNN and demonstrate the ability of quantum to improve performance even with a limited number of parameters and qubits. Wang et al. [35] achieved 100% accuracy in the binary classification of the two datasets and 90% accuracy for the UCI 10-class classification task. However, the VQC can be enhanced with QCNN, which is more immune to the Barren Plateaus (i.e., the quantum counterpart of the classical gradient vanishing problem). Moreover, more sophisticated datasets can be used for validation.

Skolik et al. [62] explored the Barren Plateaus phenomenon by monitoring the variation of the gradients when the number of qubits and the depth of the circuit (i.e., the layers) increase. Then to overcome this challenge, they design an incremental learning strategy, where the depth of the VQC increases incrementally, and only a subset of parameters are updated each step to keep the circuit at a low depth with a small number of parameters. A binary classification task is done on the MNIST dataset. Using the Layerwise learning, Skolik et al. [62] reduced the generalization error of a standard quantum network of the same size by almost 8% and demonstrated the supremacy of their approach regarding vanishing gradients when compared to similar classical DL architectures in noiseless simulations. Although the implemented circuit architecture reduces the computation time because of fast convergence, it is unsuitable for NISQ hardware.

Hossain et al. [63] proposed a system that detects malaria by classifying the blood cells. They employ the Minimum Redundancy Maximum Relevance (mRMR) and Principle Component Analysis (PCA) as feature reduction methods that optimize the contour features extracted by the Contourlet Transform method [64]. Then, they encoded the feature set to a quantum state using the ZZ feature map which is an advanced type of angle encoding that uses multiple CNOT gates and phase shift gates with the input data as angles. After that, the quantum state is entered into a VQC for binary classification. Eventually, based on the classification results a rule-based expert system determines the malaria type if the system detects a malaria disease in the red blood cells. The comparison with classical models indicates the effectiveness of the proposed approach with 99.06% accuracy.

Potempa and Porebski [65] analyzed and compared the classical and quantum approaches of image classification. The MNIST dataset is utilized for training the models. The images are reduced to  $8 \times 8$  px for both models to ensure a fair comparison. For the quantum model, the images are divided into 4 partitions of  $4 \times 4$  px. These 4 partitions are duplicated and inputted into 2 identical circuits. Each circuit consists of 4 VQCs and each VQC has 16 qubits, 16 parameterized CNOT gates with trainable weights, and one output from measuring the first qubit. The readout classical values from the 8 VQCs are concatenated and inputted into a classical output layer of 10 neurons, making the total number of parameters in the full quantum model 218 trainable parameters. At the beginning of the VQCs, the angle embedding method is employed where the image pixels are multiplied by  $\pi$  and encoded as qubits rotations. The used classical model is designed to ensure a similar number of parameters. A Multilayer Perceptron model is constructed using one input layer with 64 input nodes, one hidden layer with four neurons, and one output layer with 10 output nodes, making the number of trainable parameters 310. The trainable parameters in both models are updated using the Adam optimization method of the categorical cross-entropy loss function. The comparison confirms the superiority of quantum in terms of performance, convergence speed, and stability. The quantum model achieved an average accuracy of 70.52% with 4.45% relative percentage improvement over the classical model that resulted in 67.51% accuracy. The summary of the VQC papers are in Table 5.

**Table 5**  
Variational/Parameterized quantum circuit.

Paper	Mainly classical vs. Mainly quantum	Encoding	Dataset	Qubits	Evaluation & Results	Type	Optimizer & Cost function	Limitation
Mittal and Dana [52]	Mainly classical	Angle	LFW-Gender	4 qubits & N/A	ACC 93%	Binary	N/A & Adam	Few provided information about the encoding method, the VQC architecture, and gates.
Trochun et al. [54]	Mainly classical	Angle	Satellite Images of Hurricane Damage	2 qubits & 1 params in the VQC	ACC 72.75%	Binary	Adam/SGD & cross-entropy	Their experiments show an accuracy drop phenomena at epoch 15
Sebastianelli et al. [55]	Mainly classical	Angle	EuroSAT	4 qubits & N/A	F1 ACC Recall Precision. 97% Max ACC	Multi-class	Adam & cross-entropy	Enlarging the quantum proportion in the model and using more complex quantum circuits could be beneficial
Chalumuri et al. [57]	Mainly classical	Amplitude	UC Merced Land-Use, AID, NWPU-RESISC45	8 qubits & 1.85M params, 9 qubits & 1.92M params, and 7 qubits & 1.87M params, for the three datasets, respectively.	ACC 95.89% 86.13% 79.32% for the three datasets, respectively	Multi class	SGD & categorical cross-entropy	Did not explore other encoding methods as the amplitude encoding has high circuit depth and time complexity
Azevedo et al. [58]	Mainly classical	Angle	BCDR dataset	4 qubits & 2066 parameters in the best settings	F1 ACC Recall Precision. 84% Max ACC	Binary	Adam & cross entropy	No comparison with other embedding methods like amplitude or hybrid.
T et al. [38]	Mainly classical	Angle	MRI image	4 qubits & N/A	ACC 83.66%	Binary	Adam & cross-entropy	No comparison with the classical model to demonstrate the quantum equivalent
Wang et al. [35]	Mainly quantum	Angle Amplitude Hybrid	MNIST, UCI	6 and 10 qubits & 84-480 params	ACC & loss 100% best binary classification and 90% best ten-class classification	Binary Multi-class	Adam & Cross-entropy	Can avoid Barren Plateaus with QCNN
Skolik et al. [62]	Mainly quantum	Angle	MNIST	8 qubits & N/A	ACC 90%	Binary	Adam & Cross-entropy	The implemented circuit reduces the computation time, but it is unsuitable for NISQ hardware and it requires noiseless simulation
Hossain et al. [63]	Mainly quantum	ZZ feature map (angle)	RBC image	4 qubits & 4040 params	ACC Precision Recall Specificity. 99.17% Max ACC	Binary	N/A & Mean Squared Error (MSE)	Comparing the model with QCNN and implementing the system on real quantum hardware would enhance the study
Potempa and Porebski [65]	Mainly quantum	Angle	MNIST	Two circuits 64 qubits each & 218 total params	ACC, balanced ACC. 70.5% ACC	Multi class	Adam & cross-entropy	The number of used qubits requires high computational resources. No comparison with other encoding methods like amplitude and hybrid.

#### 4.3.2. Quantum tensor networks

A classical tensor network is a mathematical framework used to represent and manipulate large multi-dimensional arrays, known as tensors. Each tensor has a number of indices (e.g., 0 for scalar, 1 for vector, and 2 for matrix), and each index has a dimension. To combine tensors, the products of the corresponding values need to be summed over indices with a common dimension called the bond dimension. A famous example of tensor contraction is the multiplication of matrices as in (11), where the bond dimension is the dimension of the repeated index  $z$ . Each entry in  $R$  is the sum of products along the repeated index  $z$ .

$$R_{xy} = \sum_z Q_{xz} P_{zy} \quad (11)$$

Tensors are represented as nodes in the tensor network diagram, and the indices that can be used to contract tensors are represented as lines or edges that connect the nodes. Tensor networks are usually used to study complex quantum many-body systems using different architectures like Matrix Product State (MPS) [66], Multi-scale Entanglement Renormalization Ansatz (MERA) [67], and Tree Tensor Network (TTN) [68]. Moreover, tensor networks have been successfully implemented in classical machine learning classification [69,70]. Recently, researchers have started using QTN by implementing the original tensor network as quantum circuits. Fig. 12 shows how QTN can be used for image classification and how different architectures of tensor networks can be mapped to QTN using the quantum gates. First, the images are encoded and transformed to a quantum state, then

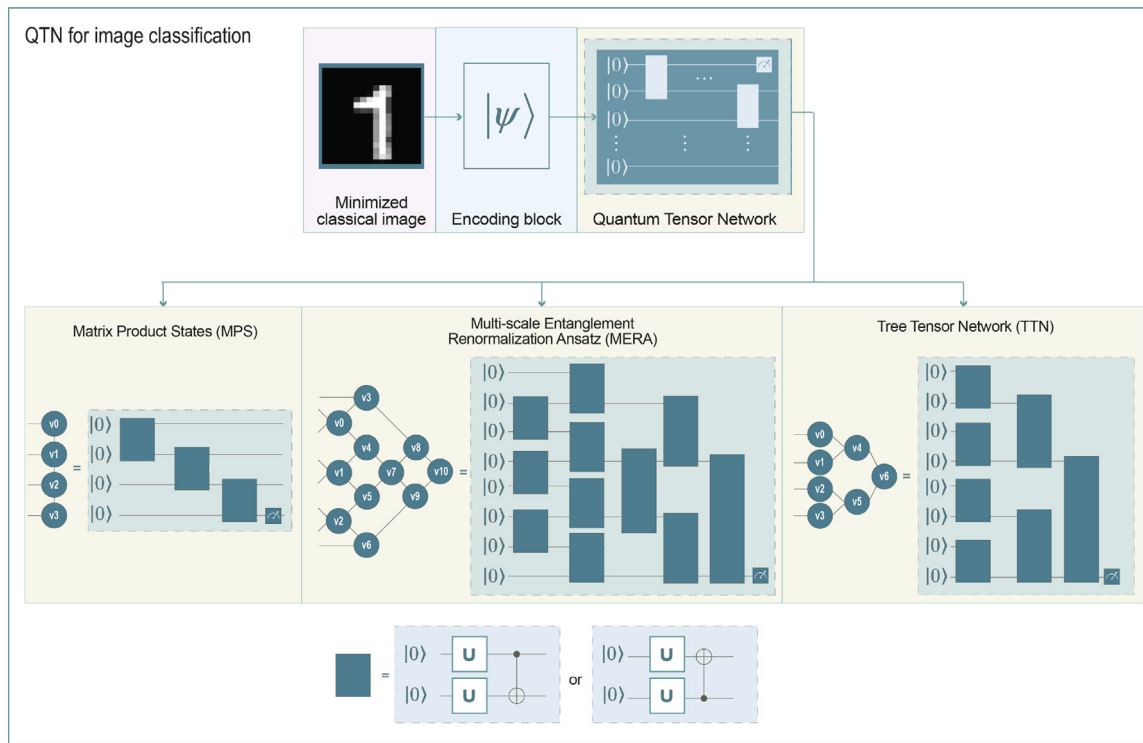


Fig. 12. Overview of QTN [71–73].

the quantum state is entered into a unique architecture of QTN, which utilizes unitary gates on each of two successive qubits to accomplish a similar connection as the original network. The unitary gates can consist of unitary gates  $U$  on individual qubits followed by CNOT gates to entangle these qubits as shown in the figure, where  $U$  can be a parameterized rotational gate.

Grant et al. [71] performed 4 binary classification tasks on the MNIST dataset. The first task is to classify 0 or 1, the second is 2 or 7, the third is odd (1, 3, 5, 7, and 9) or even (0, 2, 4, 6, and 8), and the last task is to classify numbers as  $> 4$  or  $\leq 4$ . The images are reduced to 8 pixels using PCA. These 8 pixels are encoded into 8 qubits using the angle encoding method. Grant et al. [71] created three QTN, one based on TTN architecture, the second based on the MERA architecture, and the last is a hybrid model where the gates of a MERA model are initialized with TTN pre-trained model values instead of being initialized in a completely random way. Moreover, 3 types of unitary gates are investigated which are, simple, general, and ancilla. The simple unitary is the same as the one highlighted in Fig. 12, where two rotational one-qubit gates are followed by a CNOT gate that can be implemented in both directions. The general is a two-qubit gate, and the ancilla is a three-qubit gate. Furthermore, two types of rotations are implemented in the unitary gates (complex and real rotations). All the constructed models are compared to a classical baseline logistic regression model. The study findings show that the accuracy of most constructed circuits is higher using complex rotations. Also, the MERA architecture circuits outperformed the TTN in all classification tasks and using all variations in unitary types. This indicates that increasing the number of unitary gates enhances performance. The results also indicate that general unitary gates surpassed the simple ones. In terms of comparison with the classical classifiers, all the proposed quantum models achieved higher accuracies than the logistic regression model except for those that use simple unitary gates. Overall, the MERA architecture with complex rotations and general unitary gates accomplished the highest results on three classification tasks (79.1% for  $> 4$  or  $\leq 4$ , 84.85% for odd or even, and 98.86% for 2 or 7). In the final classification task (0 or 1), the hybrid model with real rotations and general unitary type attained the highest accuracy of 99.87%.

Huang et al. [74] adjusted the approach of Grant et al. [71] and proposed a Variational Quantum Tensor Network (VQTN) following the TTN and MERA architectures. After that, they proposed the kernel encoding method and argued about its efficiency. To achieve kernel encoding, the authors standardized the data of the input dataset to have zero mean and unit standard deviation, and then they normalized each feature vector to a unit length and encoded the pixels using the angle-dense encoding method where every 2 pixels are encoded into one qubit. Another contribution of Huang et al. [74] research is the use of multiple readout qubits instead of measuring only one qubit at the end of the QTN. The experiments are done on the MNIST dataset images, which are reduced in size to 16 px and encoded into 8 qubits. The performance of the constructed models is compared to other models from previous research. Binary and multi-class classification tasks are executed in several variants of the VQTN and the QTN to compare the effects of the number of qubits and trainable parameters on the performance of quantum circuits. Also, the effect of the multiple readout qubits is investigated by comparing it to the single readout qubit, where the results show that using multiple readouts reduces the convergence time and increases the accuracy. Finally, Huang et al. [74] demonstrated the supremacy of the VQTN by outperforming previous research results and achieving almost 7% enhancement compared to the QTN with half of the qubits.

In their study, Lazzarin et al. [72] expanded on the research conducted by Grant et al. [71], this time focusing on multi-class classification. Similar to Grant et al. [71] and Lazzarin et al. [72] experimented on the MNIST dataset and examined the TTN and MERA architectures that utilized both simple and general unitary gates, as well as real and complex rotations. The MNIST images are reduced using two approaches, one is the PCA and the other is the convolutional autoencoder then the angle encoding is performed for quantum state preparation. Instead of one readout qubit, Lazzarin et al. [72] used multiple readouts like [74]. 8 qubits QTN and 2 readout qubits are selected for classifying four digits (0, 1, 2, and 3). To satisfy multi-class classification 2 approaches are proposed that depend on the type of measurement, which are qubit and amplitude decoding. The accuracy of the tests conducted

on different models showed a significant variation, ranging from 59% to 93%. This variance was due to the model architecture and the type of pre-processing used. This indicates the importance of carefully selecting the model and employing suitable data pre-processing techniques to optimize the system's performance. The best results (93%) were achieved using the autoencoder dimensionality reduction technique, the MERA architecture, the general unitaries, the complex rotations, and amplitude decoding.

Guala et al. [73] provided an overview on how to design and apply QTN to image classification tasks. They explained the circuit-cutting approach and how to apply it to MPS. Circuit-cutting is a technique to assess the performance of large quantum circuits that contain more qubits than the current quantum computers or simulators can handle. This approach is achieved by dividing the quantum circuit into smaller ones with an applicable number of qubits. Then, these circuits are executed with various configurations until the results of the different configurations are sufficient to reconstruct the full circuit output using the classical strategy. Despite its need for classical computation, this method allows for the construction of multi-qubit circuits utilizing quantum devices with limited qubits. For the image classification, Guala et al. [73] executed two image classification tasks, a simple binary classification on the bars and stripes data set, and a more complex defect detection task. For the bars and stripes data set, different image sizes are tried which are ( $4 \times 4$ ,  $16 \times 16$ , and  $256 \times 256$  px). These are encoded using the amplitude encoding method into 4, 8, and 16 qubits, respectively. Then, the TTN architecture is used as the trainable quantum circuit and the Simultaneous Perturbation Stochastic Approximation (SPSA) optimizer is utilized for training. In all the cases, 100% accuracy is accomplished because of the over-simplicity of the classification task. For the defect detection task, the authors constructed a QTN to check the severity and location of the defect in weld images. They manually selected 14 defect and 14 non-defect images and resized them to  $256 \times 256$  px. After that, a three-level approach is proposed for defect detection. In the first step, the defective images are identified using binary classification. After that, a kernel of size  $16 \times 16$  px is slid through the defective images, and each segment in the image is classified individually. In the last step, the  $1 \times 16$  defective segments are further partitioned into  $4 \times 4$  px sub-segments and these are classified again using binary classification. Eventually, by reconstructing the image from the  $4 \times 4$  segments and marking the defective segment, the location of the defects can be identified. The amplitude encoding is also utilized for this task. Three QTN based on TTN architecture are developed for the three-level classification task, the first with 16 qubits to classify the full images which resulted in 71% accuracy. Then the second with 8 qubits to classify the  $16 \times 16$  px segments and it attained 79%. Finally, the last classifier with 4 qubits for the last level classification reached 71% accuracy. Table 6 highlights the key points of the reviewed QTN papers.

#### 4.3.3. Quantum convolutional neural networks

The QCNN is the most prominent QDL approach for classifying images. QCNN is the quantum version of the classical CNN, as it also consists of multiple consecutive conv and Pooling layers. Fig. 13 compares the approaches for constructing a CNN and a QCNN [75]. As Fig. 13 illustrates, each conv layer of the QCNN contains an arbitrary 2-qubit unitary gate  $U_j$  on every successive pair of qubits, where  $j$  represents the corresponding conv layer.  $U_j$  decomposition is one of the significant decisions in constructing the QCNN. After each conv layer, the pooling layer applies single-qubit unitary gates  $V_j$  on one qubit and a measurement on the successive one. This operation decreases the number of qubits to half in each pooling layer. A few commonly used ansatzes that compose the  $U_j$  and the  $V_j$  can be found in [36,76]. Eventually, when the number of qubits is suitable after several conv and pooling layers, the FC layer of the QCNN entangles the remaining qubits with controlled gates (e.g., CNOT, CZ). Several studies in the

literature utilize and adapt the proposed QCNN architecture in [75] to the image classification task.

The research on QCNN followed mainly two approaches, the first is the implementation of a quantum conv filter to a classical circuit, and the other is to implement all classification layers as a quantum circuit of quantum conv and pooling layers.

**4.3.3.1. Quantum convolutional filter in the classical model.** Henderson et al. [78] extended the classical CNN with quantum conv filters to construct a Quanvolutional Neural Network (QuanvNN). The QuanvNN contains a quantum conv filter as the first layer, followed by six classical conv, pooling, and FC layers. A  $3 \times 3$  filter size is selected thus requiring 9 qubits to encode the pixels of the corresponding part of the image into the quantum circuit. For encoding, a simple threshold method is applied. If the value of the image pixel is greater than the threshold, the affiliated qubit has a state  $|1\rangle$ , otherwise  $|0\rangle$ . A random number of 2-qubit gates and parameterized single-qubit gates are chosen and shuffled to create one filter in the quantum layer. 1 to 50 filters are used in the experiments to determine the best filter number, which turned out to be 50. The state vector of all nine qubits is obtained using a quantum circuit simulator. The highest probability state is used to sum the measured qubits in this state and aggregate the results into one scalar value. The QuanvNN is compared to a classical CNN model. The result shows that the QuanvNN outperforms the pure classical CNN and reaches an accuracy of 95% on the MNIST dataset. The main limitation of this work is the oversimplistic encoding method that can result in data loss. Also, the model is not applicable in actual quantum hardware as it assumes the availability of the state vector of the qubits, which can never be learned in real quantum computers.

Villalba-Diez et al. [79] investigated the capability of QDL to enhance the performance of the classification of the de-scaler billets quality (i.e., bad quality or good quality). They adopted the research of Henderson et al. [78] to overcome the constraint of using the same weights in the conv window, which limits the hierarchical pre-processing by using variable weights in the edges of the  $2 \times 2$  conv window, which can adjust the significance of the image pixels. They compared the CNN F1 score with and without the benefit of the quantum filter. The key findings of this research are that the quantum filter reduces the training time and the number of epochs needed to reach the optimal weights. However, this computational improvement is a trade-off with the F1 measure, as it decreases the F1 by 0.4% and 0.2% of the good quality and bad quality classes, respectively. However, Villalba-Diez et al. [79] did not explore different ways of implementing the quantum filter to increase the F1 score.

Jing et al. [37] designed a hybrid classical-quantum CNN that classifies RGB images effectively. They constructed two ansatzes for the conv layer (i.e., Hierarchical and Flat). The experiments are conducted on the MNIST, FMNIST, and CIFAR-10 datasets using the Kunfeng cloud platform that provides large-scale simulations. 12 qubits are employed to encode the classical pixels for three channels with a window size of  $2 \times 2$ . Each qubit is represented as  $(i, j)$ , where  $i$  is the channel, and  $j$  is the pixel. Two networks are constructed with the quantum conv layer, one with two classical conv, one pooling, and two dense layers, while the other with only two dense layers. All experiments are performed on the three datasets with  $20 \times 20$  and  $10 \times 10$  px image sizes. The overall results show that the performance of the CNN with the quantum conv layer is better than pure classical CNN and the loss curves are smoother. Also, quantum CNN with larger ansatz circuits converges faster and provides higher accuracy than smaller ones. The high computation resources that are required to simulate the proposed circuits are the constraints of this method.

Easom-Mccaldin et al. [80] proposed a single-qubit QCNN. They argued about the complexity of multi-qubit circuits and the efficiency of the single-qubit encoding technique in maintaining the spatial relationship between image pixels. For encoding, a filter of size  $F \times F$  px is convolved over the image. Every time, pixels are flattened and encoded

**Table 6**  
Quantum tensor network papers.

Paper	QTN architecture	Encoding	Dataset	Qubits	Evaluation & Results	Type	Optimizer & Cost function	Limitation
Grant et al. [71]	TTN and MERA	Angle	MNIST	8 qubits	ACC, best setting achieved > 4: 79.1%, odd or even: 84.85%, 2 or 7: 98.86%, 0 or 1: 98.86%	Adam & MSE	Binary	Does not add simulated circuit noise when training the circuit. Does not achieve translation and scale invariance since no weight sharing is done within and between the layers of the models.
Huang et al. [74]	TTN and MERA	Dense Angle	MNIST	8 qubits & 18 params	ACC Recall F1 AUC. 93% average ACC	Adam & hinge loss	Binary Multi-class	Does not add simulated circuit noise when training the circuit. No comparison study with classical models.
Lazzarin et al. [72]	TTN and MERA	Angle	MNIST	8 qubits & 165 params	ACC 59%-93% depending on the architecture and the pre-processing technique	Adam & cross-entropy and MSE	Multi-class	The model noise resistance is not explored and investigated. The proposed model can only implement four class classifications since only 2 readout is performed.
Gualà et al. [73]	TTN	Amplitude	Bars and stripes. Weld Defects dataset	4, 8, and 16 qubits	100% ACC for first dataset & 71%, 79%, and 71% ACC on the three-level tasks, respectively	SPSA & custom-designed penalized loss function	Binary	Only proof-of-concept simple studies are implemented without comparing the study with other classical and quantum approaches.

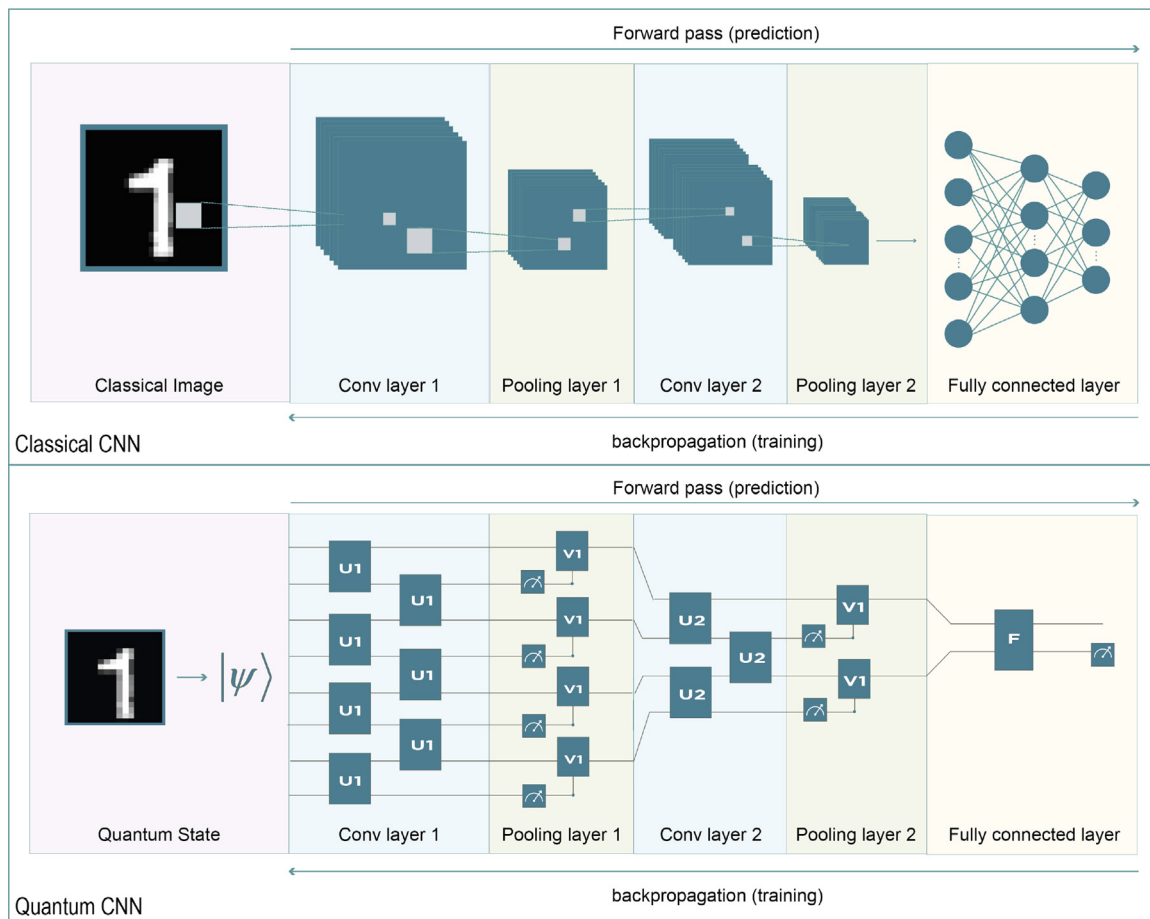


Fig. 13. The difference between CNN and QCNN [36,77].

using rotation gates on the same qubit. The process will continue until the kernel convolves the whole image from the top-left corner to the

bottom-right one. The model utilizes only six trainable parameters. These six parameters are repeatedly used on every three consecutive

pixels, where each pixel is multiplied by one parameter and added to another. After encoding, the qubit is measured, and the Adam optimizer is used to minimize the fidelity loss function between the target classes and the measured classes. For experiments, Easom-Mccaldin et al. [80] utilized subsets of grey images from MNIST, FMNIST, and ORL face datasets. Also, they investigated three filter sizes on each dataset ( $3 \times 3$ ,  $4 \times 4$ , and  $5 \times 5$ ). Overall, the results of the  $3 \times 3$  px filter outperformed the other two filters. Eventually, the proposed approach is evaluated using binary classification tasks on the MNIST, FMNIST, and ORL face datasets, which achieved 95.8%, 89.5%, and 83.3% best accuracies on each dataset, respectively. An additional 3-class classification experiment is implemented on the MNIST dataset to classify 0, 1, or 2 digits which resulted in 72.1% best accuracy. Nevertheless, Easom-Mccaldin et al. [80] did not exploit the capabilities of entanglement and multi-qubit superposition, which are the crucial aspects of quantum.

**4.3.3.2. Quantum convolutional network as the main model.** Zheng et al. [34] conducted their experiments on 1000 reduced images of the 3 and 6 classes from the MNIST dataset. After decreasing the size of the chosen images from  $28 \times 28$  px to  $8 \times 8$  px, they selected the amplitude encoding method to create the quantum state using 6 qubits for a 64 px image array. However, to overcome the time and circuit-depth constraints of the amplitude encoding (see Section 4.1.1), they proposed the Approximation Quantum State Preparation (AQSP) encoding method. During the AQSP, the amplitude encoding is used to prepare a standalone quantum circuit in a classical simulator. Let  $n$  denote the number of qubits (i.e., 6), then the suggested AQSP circuit contains 3 layers each which consists of  $9 * n R(\theta)$  gates (i.e.,  $6 * 9 * 3 = 162$ ), and  $n$  controlled-Z gates (CZ) (i.e.,  $6 * 3 = 18$ ). The full AQSP circuit uses a total of 180 gates with 3 trainable parameters to transform the amplitude encoding actual state to the  $|1\rangle^{\otimes n}$  state. Later, the primary quantum circuit starts with the  $|1\rangle^{\otimes n}$  and applies the conjugate transpose of the AQSP circuit with the saved optimal parameters to reverse the process and estimate the original quantum state. The suggested AQSP has a complexity of  $O(n)$ , which decreases the depth complexity of the amplitude encoding (i.e.,  $O(2^n)$ ). Following the state preparation, they constructed two variants of the QCNN, one for Euclidean data and the other for Non-Euclidean data. For the Euclidean data, the QCNN contains two conv and pooling layers with 54 trainable parameters. It consists of 5  $U_1$  gates in the first conv layer, 2  $U_2$  in the second conv layer, 3  $V_1$  in the first pooling layer, and a 1  $V_2$  in the second pooling layer. All  $U_j$  gates are decomposed into the same ansatz that contains  $(R_y(\theta), R_z(\theta))$  gates, and control X gates (CNOT). Likewise, all the  $V_j$  use the same PQC. The implemented FC layer uses CNOT and universal single-qubit gates to entangle the remaining two qubits. The Z expectation value  $\langle Z \rangle$  is measured on one qubit to produce the output (if  $\langle Z \rangle \geq 0$ , then the prediction belongs to the first class, otherwise to the second class). The Gradient Descent (GD), Adam, and Root Mean Squared Propagation (RMSprop) optimization methods are compared. The Stochastic Gradient Descent (SGD) is chosen as the optimizer, which calculates the gradient of the MSE loss function using the parameter-shift rule [81] to determine the optimal parameters of the circuit. Finally, they illustrated the ability of the QCNN to overcome the Barren Plateaus. Zheng et al. [34] approach achieves 96.65% accuracy. However, the main limitation of their work is that the AQSP is isolated from the QCNN process, which can be a tedious task, and it only provides an approximation of the actual state which can reduce the accuracy. Also, they do not evaluate the model with enough metrics, and the chosen numbers (i.e., 3 and 6) are not similar in shape, which may provide optimistic results. For example, classifying 2 and 5 is a more challenging task.

Huang et al. [39] proposed a Variational Convolutional Neural Network (VCNN) to replace the classical conv and pooling layers in the CNN. They employed images from the MNIST and the FMNIST datasets to perform five binary, four three-class, and two four-class classification tasks. They reduced the images to  $4 \times 4$  px and used the angle encoding

method to prepare the quantum state with a conv filter of  $2 \times 2$  px. Each  $2 \times 2$  partition of the image (i.e., 4 pixels) is multiplied by  $\pi$  to calculate the rotation angles of the  $R_y$  &  $R_z$  gates on the 4 qubits. All steps are repeated until the filter strides the full image. (i.e., four times in this case). Next, after image encoding, a superposition of all qubits is created using the Hadamard gate on each qubit, followed by a VCNN circuit that is inspired by the MERA quantum circuit. Only the quantum conv layer with successive universal 2-qubit gates  $U_j$ , the  $U_j$  is composed of  $R_x(\theta)$  gates surrounding one  $R_y(\theta)$  gate. The whole VCNN contains 48 trainable parameters. The binary-cross-entropy loss function is minimized using the SGD optimization method. Finally, for the evaluation, Huang et al. [39] compared their approach with other quantum models and used the accuracy, recall, AUC, and F1 performance metrics. The VCNN outperforms other models on all the implemented tasks. Like in Zheng et al. [34] study, no hard classification tasks are done, resulting in higher reported accuracies.

Hur et al. [36] explored different image reduction techniques as the PCA and the autoencoder. They also discussed three encoding methods (i.e., amplitude, angle, and hybrid) on the MNIST and FMNIST datasets. The hybrid encoding method consists of two types, Hybrid Angle Encoding (HAE) and Hybrid Direct Encoding (HDE). The concept behind the hybrid encoding techniques is to divide the image's feature vector into blocks and perform the encoding (i.e., angle or amplitude) for each block, which increases efficiency by reducing the depth of the circuit and the number of qubits. For the main QCNN, they implemented a similar architecture to Fig. 13 and compared the results of using 9 different ansatzes as the basic unit of the conv layers  $U$ . They demonstrated the effectiveness of QCNN with even a small number of parameters ranging from 12 to 50. The acquired results depict high performance with 99% for MNIST and 94% for FMNIST. The research can be enhanced by considering multi-class classifications. The QCNN papers are presented in Table 7.

## 5. Discussion

Quantum image classification is a hot and new research area with a promising future. Fig. 14 shows the yearly publication of the reviewed papers from 2015 to 2022. Quantum image classification papers are increasing every year. The massive expansion in the paper count indicates that quantum image classification may reach a practical and realistic point with the researcher's considerable efforts and interest in the field. It also signifies the need for additional analysis to bridge the existing gaps and contribute to the current studies by addressing some of the challenges in the area.

### 5.1. Key challenges

#### 5.1.1. Noisy intermediate scale quantum

In the NISQ era, quantum computers contain a limited number of noisy qubits. These limitations challenge the complex quantum circuits and classifiers and limit the size of classical images that can be encoded into the quantum state and the number of trainable parameters in the PQC. The constraints of near-term quantum computers make some people doubt the benefits of these machines in industrial and real-world applications [13]. Most of the experiments in the discussed papers are executed in fault-tolerant simulators that do not consider the noise in real quantum computers, which questions whether the NISQ computers are capable of actually classifying images.

#### 5.1.2. Limited number of feasible simulated qubits

The exponential growth of parameters that simulators need to keep track of with the number of qubits limits the number of feasible qubits in the simulators. (e.g., for 100 qubits, the simulator has to operate with  $1.26 * 10^{30}$  amplitudes, which is a massive number). This constraint restricts the QML and QDL in the image classification tasks due to the large number of pixels that images contain. Moreover, because of this hurdle, researchers are driven to employ image reduction methods that result in immense information loss and accuracy drop.

**Table 7**  
QCNN papers.

Paper	Filter vs. main	Encoding	Dataset	Qubits & Params	Evaluation & Results	Type	Optimizer & Cost function	Limitation
Henderson et al. [78]	Filter	Threshold	MNIST	9 qubits	ACC 95%	Multi-class	N/A & log-loss	Oversimplistic encoding method & Assumes the availability of the state vector of the qubits
Villalba-Diez et al. [79]	Filter	Angle	descaler billets quality	4 qubits	F1 96.8% for good class & 96.0% for bad class	Binary	Adam & sparse categorical cross-entropy	No exploration of different implementations and sizes of the quantum filter as they only used a $2 \times 2$ conv filter that did not outperform the classical F1 score.
Jing et al. [37]	Filter	Angle	MNIST, FMNIST, CIFAR-10	12 qubits	ACC, loss. various results	Multi-class	GD & cross-entropy	High computation resources are needed to meet the requirements of the used qubit number and circuit complexity
Easom-Mccaldin et al. [80]	Filter	Angle Single-qubit	MNIST, FMNIST, ORL face	1 qubit & min 6 params	ACC & loss. For binary: 95.8% on MNIST 89.5% on FMNIST 83.3% on ORL face. For 3-class: 72.1% on MNIST	Binary Multi-class	Adam & fidelity	Using one qubit prevents the exploitation of the capabilities of entanglement and multi-qubit superposition
Zheng et al. [34]	Main	Amplitude AQSP	MNIST	6 qubits & 54 params	ACC 96.65%	Binary	SGD, Adam, RMSprop, GD & MSE	AQSP is isolated from the QCNN process, which can be a tedious task. Only provides an approximation of the actual state, which can reduce the accuracy.
Hur et al. [36]	Main	Amplitude, Angle, Dense, HAE, HDE	MNIST, FMNIST	8 qubits & 12-51 params	ACC 63%-98%	Binary	Adam and Nesterov moment & MSE and Cross entropy	No multi-classification support. Does not contain noise resistance investigation with a noisy simulator or real quantum hardware
Huang et al. [39]	Main	Angle	MNIST, FMNIST	4 qubits & 48 params	ACC, Recall, F1, AUC. 92.5%-99.9% depending on the task	Binary Multi-class	SGD & cross-entropy	No hard classification tasks like classifying 2 and 5, resulting in higher reported accuracies.

### 5.1.3. Image encoding methods

One of the critical challenges in quantum image classification is image embedding. Researchers are still deriving more advanced and novel hybrid encoding methods; however, until now, all the embedding methods require image down-scaling mainly because of the considerable depth of the circuit or the number of qubits, as discussed in Section 4.1. The NISQ and qubit limitations make image encoding methods the most significant decision for an effective quantum image classification model.

### 5.1.4. Color images

Only a few studies adopt the QML and QDL for color image classification like RGB images. The models used in these studies are mainly classical and they contain CNN layers that facilitate the feature extraction of RGB images. Nevertheless, in the mainly quantum models, fewer studies incorporate RGB arrays because that would require triple the qubit number.

### 5.1.5. Sophisticated images datasets

As with the color images, only the models that use large classical portions succeed in classifying more advanced datasets and utilizing the quantum circuits for more important tasks.

### 5.2. Future directions

Fig. 15 reports the number of surveyed papers, the number of papers that support color, and the number of papers that implement multi-class classification for each algorithm type. The statistics show a lack of literature supporting color and multi-class classification and indicate the necessity for new research that addresses these issues.

#### 5.2.1. Novel image embedding

Several encoding techniques have been proposed and adopted in the literature to embed classical images into quantum states. However, there is still a gap for an efficient encoding method that adapts sufficiently to the available number of qubits and hence enables the use of the size of the original images without the need for image down-sizing.

#### 5.2.2. RGB support

An encoding method for RGB images can result in a considerable contribution. The red, green, and blue channels can be extracted and encoded separately using a novel approach, and the CIFAR-10 and CIFAR-100 datasets can be utilized for the experiments.

#### 5.2.3. Quantum image classification for essential applications

Adapting the quantum image classification for more essential tasks is another recommendation since the statistics of the reviewed papers reveal that only three studies used the quantum for medical

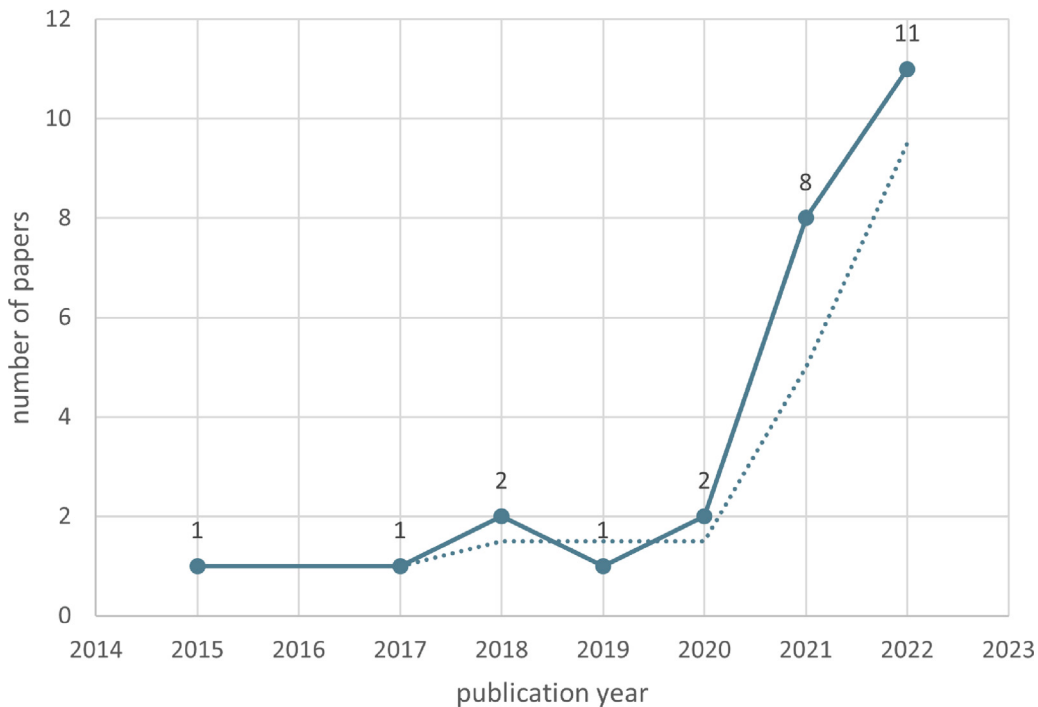


Fig. 14. The years of the reviewed paper publication.

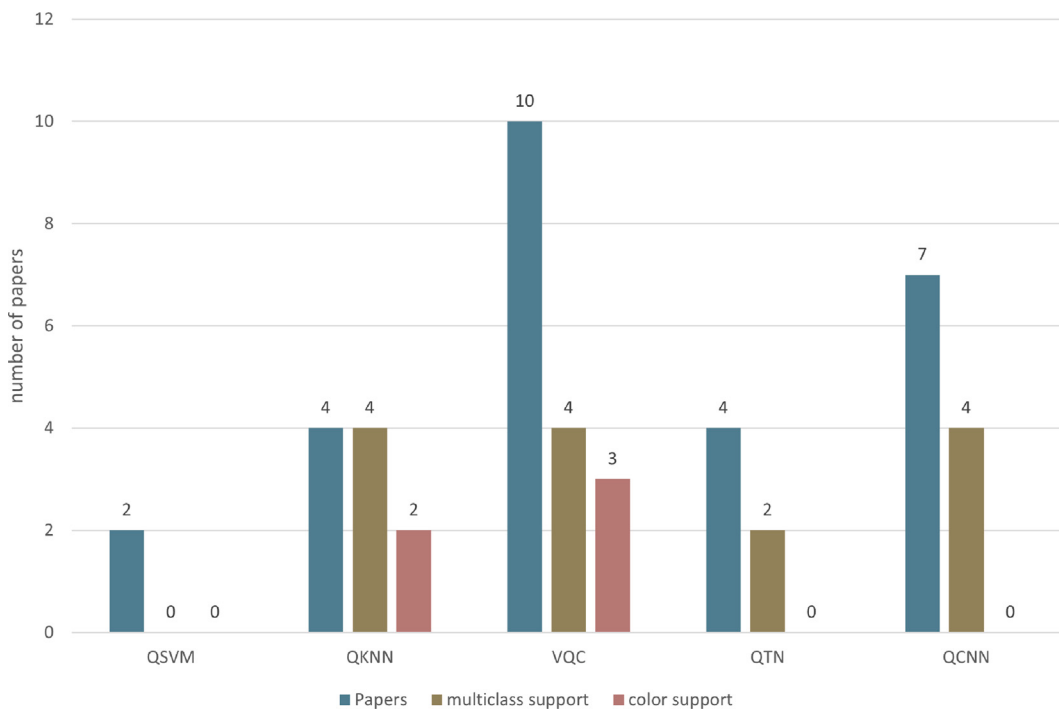


Fig. 15. Color and multi-class support in the reviewed papers.

fields [38,58,63]. Another future direction may be constructing additional ansatzes and PQCs and comparing their performance for specific image classification tasks.

## 6. Conclusion

Quantum image classification is a new domain with rising interest among researchers. It holds significance and promising capabilities to improve the computational cost of classical image classification

algorithms. The rising number of recent research papers and the lack of a comprehensive survey motivate this review paper. This research summarizes 27 papers related to QML and QDL in image classification, which are collected from the top research databases. It provides summary tables, adopts an easy-to-follow organization with a unique taxonomy, and illustrates the general models and approaches with several figures. In addition, it discusses the pros and cons of angle and amplitude embedding with real experiments. Also, it highlights the limitations of each paper. Moreover, it divides the summarized

research based on the used techniques and a unique taxonomy into QML (i.e., QSVM and QKNN) and QDL (i.e., VQC, QTN, and QCNN). Furthermore, the study suggests some critical challenges, such as the limited scalability of quantum to large and sophisticated images and datasets and the lack of color support. Finally, the research highlights future directions based on the gaps in the literature, such as creating novel quantum encoding methods, investigating new quantum ansatz architectures, and employing quantum in essential fields like medical studies.

### CRediT authorship contribution statement

**Ruba Kharsa:** Investigation, Writing – original draft. **Ahmed Bouridane:** Conceptualization, Validation, Reviewing & editing. **Abbes Amira:** Supervision, Validation, Reviewing & editing.

### Declaration of competing interest

The authors declare that they have no known competing financial interests or personal relationships that could have appeared to influence the work reported in this paper.

### Data availability

No data was used for the research described in the article.

### References

- [1] S. Pattanayak, Quantum Machine Learning with Python : Using Cirq from Google Research and IBM Qiskit, 2021.
- [2] R. Rietsche, C. Dremel, S. Bosch, L. Steinacker, M. Meckel, J.-M. Leimeister, Quantum computing, Electron. Mark. 32 (4) (2022) 2525–2536, <http://dx.doi.org/10.1007/s12525-022-00570-y>.
- [3] A.J. Daley, I. Bloch, C. Kokail, S. Flannigan, N. Pearson, M. Troyer, P. Zoller, Practical quantum advantage in quantum simulation, Nature 607 (7920) (2022) 667–676, <http://dx.doi.org/10.1038/s41586-022-04940-6>.
- [4] P.B. Upama, M.J.H. Faruk, M. Nazim, M. Masum, H. Shahriar, G. Uddin, S. Barzanjeh, S.I. Ahamed, A. Rahman, Evolution of quantum computing: A systematic survey on the use of quantum computing tools, in: 2022 IEEE 46th Annual Computers, Software, and Applications Conference (COMPSAC), 2022, pp. 520–529, <http://dx.doi.org/10.1109/COMPSAC54236.2022.00096>.
- [5] E. Goceri, Challenges and recent solutions for image segmentation in the era of deep learning, in: 2019 Ninth International Conference on Image Processing Theory, Tools and Applications (IPTA), 2019, pp. 1–6, <http://dx.doi.org/10.1109/IPTA.2019.8936087>.
- [6] W. Rawat, Z. Wang, Deep convolutional neural networks for image classification: A comprehensive review, Neural Comput. 29 (9) (2017) 2352–2449.
- [7] Z.-Q. Zhao, P. Zheng, S.-t. Xu, X. Wu, Object detection with deep learning: A review, IEEE Trans. Neural Netw. Learn. Syst. 30 (11) (2019) 3212–3232.
- [8] C.A. Mack, Fifty years of Moore's law, IEEE Trans. Semicond. Manuf. 24 (2) (2011) 202–207.
- [9] M. Schuld, I. Sinayskiy, F. Petruccione, An introduction to quantum machine learning, Contemp. Phys. 56 (2) (2015) 172–185.
- [10] A.K. Malviya, N. Tiwari, M. Chawla, Quantum cryptanalytic attacks of symmetric ciphers: A review, Comput. Electr. Eng. 101 (2022) 108122, <http://dx.doi.org/10.1016/j.compeleceng.2022.108122>, URL: <https://www.sciencedirect.com/science/article/pii/S0045790622003743>.
- [11] S.B. Ramezani, A. Sommers, H.K. Manchukonda, S. Rahimi, A. Amirlatifi, Machine learning algorithms in quantum computing: A survey, in: 2020 International Joint Conference on Neural Networks (IJCNN), 2020, pp. 1–8, <http://dx.doi.org/10.1109/IJCNN48605.2020.9207714>.
- [12] F. Ablayev, M. Ablayev, J.Z. Huang, K. Khadiev, N. Salikhova, D. Wu, On quantum methods for machine learning problems part I: Quantum tools, Big Data Min. Anal. 3 (1) (2020) 41–55, <http://dx.doi.org/10.26599/BDMA.2019.9020016>.
- [13] M. Avramouli, I. Savvas, G. Garani, A. Vasilaki, Quantum machine learning: Current state and challenges, in: 25th Pan-Hellenic Conference on Informatics, in: PCI 2021, Association for Computing Machinery, New York, NY, USA, 2021, pp. 397–402, <http://dx.doi.org/10.1145/3503823.3503896>, URL: <https://doi.org/10.1145/3503823.3503896>.
- [14] V.R. Satuluri, V. Ponnusamy, Quantum-enhanced machine learning, in: 2021 Smart Technologies, Communication and Robotics (STCR), 2021, pp. 1–6, <http://dx.doi.org/10.1109/STCR51658.2021.9589016>.
- [15] G.S. Uehara, A. Spanias, W. Clark, Quantum information processing algorithms with emphasis on machine learning, in: 2021 12th International Conference on Information, Intelligence, Systems & Applications (IISA), 2021, pp. 1–11, <http://dx.doi.org/10.1109/IISA52424.2021.9555570>.
- [16] E.H. Houssein, Z. Abohashima, M. Elhoseny, W.M. Mohamed, Machine learning in the quantum realm: The state-of-the-art, challenges, and future vision, Expert Syst. Appl. 194 (2022) 116512, <http://dx.doi.org/10.1016/j.eswa.2022.116512>, URL: <https://www.sciencedirect.com/science/article/pii/S0957417422000136>.
- [17] D. Maheshwari, B. Garcia-Zapirain, D. Sierra-Sosa, Quantum machine learning applications in the biomedical domain: A systematic review, IEEE Access 10 (2022) 80463–80484, <http://dx.doi.org/10.1109/ACCESS.2022.3195044>.
- [18] Y. Li, M. Tian, G. Liu, C. Peng, L. Jiao, Quantum optimization and quantum learning: A survey, IEEE Access 8 (2020) 23568–23593, <http://dx.doi.org/10.1109/ACCESS.2020.2970105>.
- [19] M.A. Serrano, J.A. Cruz-Lemus, R. Pérez-Castillo, M. Piattini, Quantum software components and platforms: Overview and quality assessment, ACM Comput. Surv. (2022) <http://dx.doi.org/10.1145/3548679>.
- [20] C. Lu, S. Kundu, A. Arunachalam, K. Basu, Survey on quantum noise-aware machine learning, in: 2022 IEEE 15th Dallas Circuit and System Conference (DCAS), 2022, pp. 1–2, <http://dx.doi.org/10.1109/DCAS53974.2022.9845619>.
- [21] N. Abura'ed, F.S. Khan, H. Bhaskar, Advances in the quantum theoretical approach to image processing applications, ACM Comput. Surv. 49 (4) (2017) <http://dx.doi.org/10.1145/3009965>, URL: <https://doi.org/uoseresources.remotexs.xyz/10.1145/3009965>.
- [22] F. Yan, A.M. Ilyas, S.E. Venegas-Andraca, A survey of quantum image representations, Quantum Inf. Process. 15 (1) (2016) 1–35, <http://dx.doi.org/10.1007/s11128-015-1195-6>.
- [23] S. Chakraborty, S.B. Mandal, S.H. Shaikh, Quantum image processing: challenges and future research issues, Int. J. Inf. Technol. 14 (1) (2022) 475–489, <http://dx.doi.org/10.1007/s41870-018-0227-8>.
- [24] S. Kundu, S. Ghosh, Security aspects of quantum machine learning: Opportunities, threats and defenses, in: Proceedings of the Great Lakes Symposium on VLSI 2022, GLSVLSI '22, Association for Computing Machinery, New York, NY, USA, 2022, pp. 463–468, <http://dx.doi.org/10.1145/3526241.3530833>, URL: <https://doi.org/uoseresources.remotexs.xyz/10.1145/3526241.3530833>.
- [25] M.A. Metawei, H. Said, M. Taher, H. Eldeib, S.M. Nassar, Survey on hybrid classical-quantum machine learning models, in: 2020 International Conference on Communications, Computing, Cybersecurity, and Informatics (CCCI), 2020, pp. 1–6, <http://dx.doi.org/10.1109/CCCI49893.2020.9256649>.
- [26] D. Huang, M. Wang, J. Wang, J. Yan, A survey of quantum computing hybrid applications with brain-computer interface, Cogn. Robot. 2 (2022) 164–176, <http://dx.doi.org/10.1016/j.cogr.2022.07.002>, URL: <https://www.sciencedirect.com/science/article/pii/S2667241322000155>.
- [27] W. Li, D.-L. Deng, Recent advances for quantum classifiers, Sci. China Phys. Mech. Astron. 65 (2) (2021) 220301, <http://dx.doi.org/10.1007/s11433-021-1793-6>.
- [28] R.K. Nath, H. Thapliyal, T.S. Humble, A review of machine learning classification using quantum annealing for real-world applications, SN Comput. Sci. 2 (5) (2021) 365, <http://dx.doi.org/10.1007/s42979-021-00751-0>.
- [29] R. Tumulka, Dirac notation, in: D. Greenberger, K. Hentschel, F. Weinert (Eds.), Compendium of Quantum Physics, Springer Berlin Heidelberg, Berlin, Heidelberg, 2009, pp. 172–174, [http://dx.doi.org/10.1007/978-3-540-70626-7\\_55](http://dx.doi.org/10.1007/978-3-540-70626-7_55).
- [30] D. Copsey, M. Oskin, F. Impens, T. Metodiev, A. Cross, F. Chong, I. Chuang, J. Kubiatowicz, Toward a scalable, silicon-based quantum computing architecture, IEEE J. Sel. Top. Quantum Electron. 9 (6) (2003) 1552–1569, <http://dx.doi.org/10.1109/JSTQE.2003.820922>.
- [31] M. Benedetti, E. Lloyd, S. Sack, M. Fiorentini, Parameterized quantum circuits as machine learning models, Quantum Sci. Technol. 4 (4) (2019) 043001.
- [32] L. Deng, The mnist database of handwritten digit images for machine learning research, IEEE Signal Process. Mag. 29 (6) (2012) 141–142.
- [33] D.K. Park, F. Petruccione, J.-K.K. Rhee, Circuit-based quantum random access memory for classical data, Sci. Rep. 9 (1) (2019) <http://dx.doi.org/10.1038/s41598-019-40439-3>, Cited by: 46; All Open Access, Gold Open Access, Green Open Access.
- [34] J. Zheng, Q. Gao, J. Lü, M. Ogorzałek, Y. Pan, Y. Lü, Design of a quantum convolutional neural network on quantum circuits, J. Franklin Inst. B (2022) <http://dx.doi.org/10.1016/j.jfranklin.2022.07.033>, URL: <https://www.sciencedirect.com/science/article/pii/S0016003222005166>.
- [35] Y. Wang, Y. Wang, C. Chen, R. Jiang, W. Huang, Development of variational quantum deep neural networks for image recognition, Neurocomputing 501 (2022) 566–582, <http://dx.doi.org/10.1016/j.neucom.2022.06.010>, URL: <https://www.sciencedirect.com/science/article/pii/S0925231222007275>.
- [36] T. Hur, L. Kim, D.K. Park, Quantum convolutional neural network for classical data classification, Quantum Mach. Intell. 4 (1) (2022) 3, <http://dx.doi.org/10.1007/s42484-021-00061-x>.
- [37] Y. Jing, X. Li, Y. Yang, C. Wu, W. Fu, W. Hu, Y. Li, H. Xu, RGB image classification with quantum convolutional ansatz, Quantum Inf. Process. 21 (3) (2022) 101, <http://dx.doi.org/10.1007/s11128-022-03442-8>.

- [38] K. T, S. S, T.S. Manikumar, T. Dheeraj, A. Sumanth, Brain tumor recognition based on classical to quantum transfer learning, in: 2022 International Conference on Innovative Trends in Information Technology (ICITIIT), 2022, pp. 1–5, <http://dx.doi.org/10.1109/ICITIIT54346.2022.9744220>.
- [39] F. Huang, X. Tan, R. Huang, Q. Xu, Variational convolutional neural networks classifiers, *Physica A* 605 (2022) 128067, <http://dx.doi.org/10.1016/j.physa.2022.128067>, URL: <https://www.sciencedirect.com/science/article/pii/S0378437122006641>.
- [40] B. Ville, I. Josh, S. Maria, G. Christian, B. Carsten, M. Keri, K. Nathan, PennyLane: Automatic differentiation of hybrid quantum-classical computations, 2022, [arXiv:1811.04968](https://arxiv.org/abs/1811.04968).
- [41] M. Mottonen, J.J. Virtiaainen, V. Bergholm, M.M. Salomaa, Transformation of quantum states using uniformly controlled rotations, 2004, arXiv preprint [quant-ph/0407010](https://arxiv.org/abs/quant-ph/0407010).
- [42] A. Delibasic, G. Cavallaro, M. Willsch, F. Melgani, M. Riedel, K. Michielsen, Quantum support vector machine algorithms for remote sensing data classification, in: 2021 IEEE International Geoscience and Remote Sensing Symposium (IGARSS), 2021, pp. 2608–2611, <http://dx.doi.org/10.1109/IGARSS47720.2021.9554802>.
- [43] R. Roscher, M. Volpi, C. Mallet, L. Drees, J.D. Wegner, SemCity Toulouse: A benchmark for building instance segmentation in satellite images, in: ISPRS Annals of Photogrammetry, Remote Sensing and Spatial Information Sciences, Vol. 5, 2020, pp. 109–116.
- [44] C.C. McGeoch, Adiabatic quantum computation and quantum annealing: Theory and practice, *Synth. Lect. Quantum Comput.* 5 (2) (2014) 1–93.
- [45] Z. Li, X. Liu, N. Xu, J. Du, Experimental realization of a quantum support vector machine, *Phys. Rev. Lett.* 114 (2015) 140504, <http://dx.doi.org/10.1103/PhysRevLett.114.140504>, URL: <https://link.aps.org/doi/10.1103/PhysRevLett.114.140504>.
- [46] A. Rana, P. Vaidya, G. Gupta, A comparative study of quantum support vector machine algorithm for handwritten recognition with support vector machine algorithm, *Mater. Today: Proc.* 56 (2022) 2025–2030, <http://dx.doi.org/10.1016/j.matpr.2021.11.350>, URL: <https://www.sciencedirect.com/science/article/pii/S221478532107327>. International Conference on Applied Research and Engineering 2021.
- [47] Y. Ruan, X. Xue, H. Liu, J. Tan, X. Li, Quantum algorithm for K-nearest neighbors classification based on the metric of hamming distance, *Internat. J. Theoret. Phys.* 56 (11) (2017) 3496–3507, <http://dx.doi.org/10.1007/s10773-017-3514-4>.
- [48] Y. Dang, N. Jiang, H. Hu, Z. Ji, W. Zhang, Image classification based on quantum K-Nearest-Neighbor algorithm, *Quantum Inf. Process.* 17 (9) (2018) 239, <http://dx.doi.org/10.1007/s11128-018-2004-9>.
- [49] Y. Wang, R. Wang, D. Li, D. Adu-Gyamfi, K. Tian, Y. Zhu, Improved handwritten digit recognition using quantum k-nearest neighbor algorithm, *Internat. J. Theoret. Phys.* 58 (7) (2019) 2331–2340.
- [50] N.-R. Zhou, X.-X. Liu, Y.-L. Chen, N.-S. Du, Quantum K-nearest-neighbor image classification algorithm based on K-L transform, *Internat. J. Theoret. Phys.* 60 (3) (2021) 1209–1224, <http://dx.doi.org/10.1007/s10773-021-04747-7>.
- [51] J. Gou, L. Du, Y. Zhang, T. Xiong, et al., A new distance-weighted k-nearest neighbor classifier, *J. Inf. Comput. Sci.* 9 (6) (2012) 1429–1436.
- [52] S. Mittal, S.K. Dana, Gender recognition from facial images using hybrid classical-quantum neural network, in: 2020 IEEE Students Conference on Engineering & Systems (SCES), 2020, pp. 1–6, <http://dx.doi.org/10.1109/SCES50439.2020.9236711>.
- [53] K. Simonyan, A. Zisserman, Very deep convolutional networks for large-scale image recognition, 2014, arXiv preprint [arXiv:1409.1556](https://arxiv.org/abs/1409.1556).
- [54] Y. Trochun, Z. Wang, O. Rokovy, G. Peng, O. Alienin, G. Lai, Y. Gordienko, S. Stirenko, Hurricane damage detection by classic and hybrid classic-quantum neural networks, in: 2021 International Conference on Space-Air-Ground Computing (SAGC), 2021, pp. 152–156, <http://dx.doi.org/10.1109/SAGC52752.2021.00033>.
- [55] A. Sebastianelli, D.A. Zaidenberg, D. Spiller, B.L. Saux, S.L. Ullo, On circuit-based hybrid quantum neural networks for remote sensing imagery classification, *IEEE J. Sel. Top. Appl. Earth Obs. Remote Sens.* 15 (2022) 565–580, <http://dx.doi.org/10.1109/JSTARS.2021.3134785>.
- [56] P. Helber, B. Bischke, A. Dengel, D. Borth, Introducing eurosat: A novel dataset and deep learning benchmark for land use and land cover classification, in: IGARSS 2018 - 2018 IEEE International Geoscience and Remote Sensing Symposium, 2018, pp. 204–207, <http://dx.doi.org/10.1109/IGARSS.2018.8519248>.
- [57] A. Chalamuri, R. Kune, S. Kannan, B. Manoj, Quantum-enhanced deep neural network architecture for image scene classification, *Quantum Inf. Process.* 20 (11) (2021) 1–21.
- [58] V. Azevedo, C. Silva, I. Dutra, Quantum transfer learning for breast cancer detection, *Quantum Mach. Intell.* 4 (1) (2022) 5, <http://dx.doi.org/10.1007/s42484-022-00062-4>.
- [59] G. Huang, Z. Liu, L. Van Der Maaten, K.Q. Weinberger, Densely connected convolutional networks, in: Proceedings of the IEEE Conference on Computer Vision and Pattern Recognition, 2017, pp. 4700–4708.
- [60] K. He, X. Zhang, S. Ren, J. Sun, Deep residual learning for image recognition, in: Proceedings of the IEEE Conference on Computer Vision and Pattern Recognition, 2016, pp. 770–778.
- [61] S. Xie, R. Girshick, P. Dollár, Z. Tu, K. He, Aggregated residual transformations for deep neural networks, in: Proceedings of the IEEE Conference on Computer Vision and Pattern Recognition, 2017, pp. 1492–1500.
- [62] A. Skolik, J.R. McClean, M. Mohseni, P. van der Smagt, M. Leib, Layerwise learning for quantum neural networks, *Quantum Mach. Intell.* 3 (2021) 1–11.
- [63] M.M. Hossain, M.A. Rahim, A.N. Bahar, M.M. Rahman, Automatic malaria disease detection from blood cell images using the variational quantum circuit, *Inform. Med. Unlocked* 26 (2021) 100743, <http://dx.doi.org/10.1016/j.imu.2021.100743>, URL: <https://www.sciencedirect.com/science/article/pii/S2352914821002197>.
- [64] M.N. Do, M. Vetterli, The contourlet transform: an efficient directional multiresolution image representation, *IEEE Trans. Image Process.* 14 (12) (2005) 2091–2106.
- [65] R. Potempa, S. Porebski, Comparing concepts of quantum and classical neural network models for image classification task, in: M. Choraś, R.S. Choraś, M. Kurzyński, P. Trajdos, J. Pejaś, T. Hyla (Eds.), *Progress in Image Processing, Pattern Recognition and Communication Systems*, Springer International Publishing, Cham, 2022, pp. 61–71.
- [66] R. Orús, A practical introduction to tensor networks: Matrix product states and projected entangled pair states, *Ann. Physics* 349 (2014) 117–158, <http://dx.doi.org/10.1016/j.aop.2014.06.013>, URL: <https://www.sciencedirect.com/science/article/pii/S0003491614001596>.
- [67] G. Evenbly, G. Vidal, Tensor network states and geometry, *J. Stat. Phys.* 145 (2011) 891–918.
- [68] V. Murg, F. Verstraete, Ö. Legeza, R.M. Noack, Simulating strongly correlated quantum systems with tree tensor networks, *Phys. Rev. B* 82 (20) (2010) 205105.
- [69] R. Selvan, E.B. Dam, Tensor networks for medical image classification, in: *Medical Imaging with Deep Learning*, PMLR, 2020, pp. 721–732.
- [70] G. Chen, Q. Chen, X. Zhu, Y. Chen, Z. Yuan, Tensor network for image classification, in: 2020 8th International Conference on Digital Home (ICDH), 2020, pp. 135–140, <http://dx.doi.org/10.1109/ICDH51081.2020.00031>.
- [71] E. Grant, M. Benedetti, S. Cao, A. Hallam, J. Lockhart, V. Stojevic, A.G. Green, S. Severini, Hierarchical quantum classifiers, *npj Quantum Inf.* 4 (1) (2018) 65.
- [72] M. Lazzarin, D.E. Galli, E. Prati, Multi-class quantum classifiers with tensor network circuits for quantum phase recognition, *Phys. Lett. A* 434 (2022) 128056, <http://dx.doi.org/10.1016/j.physleta.2022.128056>, URL: <https://www.sciencedirect.com/science/article/pii/S0375960122001384>.
- [73] D. Gualà, S. Zhang, E. Cruz, C.A. Riofrío, J. Klepsch, J.M. Arrazola, Practical overview of image classification with tensor-network quantum circuits, *Sci. Rep.* 13 (1) (2023) 4427.
- [74] R. Huang, X. Tan, Q. Xu, Variational quantum tensor networks classifiers, *Neurocomputing* 452 (2021) 89–98, <http://dx.doi.org/10.1016/j.neucom.2021.04.074>, URL: <https://www.sciencedirect.com/science/article/pii/S092523122100624X>.
- [75] I. Cong, S. Choi, M.D. Lukin, Quantum convolutional neural networks, *Nat. Phys.* 15 (12) (2019) 1273–1278, <http://dx.doi.org/10.1038/s41567-019-0648-8>.
- [76] V.V. Shende, I.L. Markov, S.S. Bullock, Minimal universal two-qubit controlled-NOT-based circuits, *Phys. Rev. A* 69 (2004) 062321, <http://dx.doi.org/10.1103/PhysRevA.69.062321>, URL: <https://link.aps.org/doi/10.1103/PhysRevA.69.062321>.
- [77] Y. Lü, Q. Gao, J. Lü, M. Ogorzałek, J. Zheng, A quantum convolutional neural network for image classification, in: 2021 40th Chinese Control Conference (CCC), 2021, pp. 6329–6334, <http://dx.doi.org/10.23919/CCC52363.2021.9550027>.
- [78] M. Henderson, S. Shakya, S. Pradhan, T. Cook, Quanvolutional neural networks: powering image recognition with quantum circuits, *Quantum Mach. Intell.* 2 (1) (2020) 2, <http://dx.doi.org/10.1007/s42484-020-00012-y>.
- [79] J. Villalba-Diez, J. Ordieres-Meré, A. González-Marcos, A.S. Larzabal, Quantum deep learning for steel industry computer vision quality control, *IFAC-PapersOnLine* 55 (2) (2022) 337–342, <http://dx.doi.org/10.1016/j.ifacol.2022.04.216>, URL: <https://www.sciencedirect.com/science/article/pii/S2405896322002178>. 14th IFAC Workshop on Intelligent Manufacturing Systems IMS 2022.
- [80] P. Easom-Mccaldin, A. Bouridane, A. Belatreche, R. Jiang, On depth, robustness and performance using the data re-uploading single-qubit classifier, *IEEE Access* 9 (2021) 65127–65139, <http://dx.doi.org/10.1109/ACCESS.2021.3075492>.
- [81] K. Mitarai, M. Negoro, M. Kitagawa, K. Fujii, Quantum circuit learning, *Phys. Rev. A* 98 (2018) 032309, <http://dx.doi.org/10.1103/PhysRevA.98.032309>, URL: <https://link.aps.org/doi/10.1103/PhysRevA.98.032309>.

**Ruba Kharsa** received her B.Sc. degree in computer science and engineering from Al Ghurair University in 2019. She is now pursuing her M.Sc. studies in computer science at the University of Sharjah. Her research interests include machine learning, artificial intelligence, natural language processing, and quantum computing.



**Ahmed Bouridane** (Senior Member, IEEE) received an “Ingenieur d’Etat” degree in electronics from “Ecole Nationale Polytechnique” of Algiers (ENPA), Algeria, in 1982, an M.Phil. degree in electrical engineering (VLSI design for signal processing) from the University of Newcastle-Upon-Tyne, U.K., in 1988, and a Ph.D. degree in electrical engineering (computer vision) from the University of Nottingham, U.K., in 1992. From 1992 to 1994, he worked as a research developer in telesurveillance and access control applications. In 1994, he joined Queen’s University Belfast, U.K., initially as Lecturer in computer architecture and image processing and later on he was promoted to reader in computer science. In 2009, he joined Northumbria University at Newcastle leading the Computational Intelligence and Visual Computing Lab. His is now a professor of machine intelligence and director of the Cybersecurity and Data Analytics Research Center at the University of Sharjah, UAE. His research interests are in machine learning with applications to imaging for forensics and security, quantitative pathology and biomedical engineering, homeland security and video analytics. He has authored and co-authored more than 350 publications and three research books on imaging for forensics and security and biometric security and privacy.



**Abbes Amira** (Senior Member, IEEE) received the Ph.D. degree in 2001 from Queen’s University Belfast, U.K. Since then, he has taken many academic and consultancy positions in the United Kingdom, Europe, Asia, and the Middle East. He is currently the Dean of the College of Computing and Informatics at the University of Sharjah, U.A.E., He has taken visiting professor positions at the University of Tun Hussein Onn, Malaysia and the University of Nancy, Henri Poincaré, France. He has also conducted consultancy services for several government agencies and companies in the private sector. During his career to date, he has been successful in securing substantial funding from government agencies and industry; he has supervised more than 25 Ph.D. students and has over 400 publications in top journals and conferences in the area of embedded systems, the IoT, and image and signal processing. He obtained many international awards, including the 2008 VARIAN prize offered by the Swiss Society of Radiobiology and Medical Physics, CAST Award, DELL-EM Envision the Future (2018), IET Premium Award (2017), and many best paper and recognition awards in IEEE international conferences and events., Prof. Amira’s research interests include artificial intelligence, embedded systems, high-performance computing, big data and the IoT, connected health, image and vision systems, and biometrics and security. He has participated as Guest Editor and member of the editorial board in many international journals including recent special issues in IEEE Internet of Things Journal and Pattern Recognition (Elsevier). He is a Fellow of IET, Fellow of the Higher Education Academy, and a Senior Member of ACM.